NASA TECHNICAL NOTE

NASA TN D-5005

C. 1

NASA TN D-5005

LARGE-SCALE WIND-TUNNEL INVESTIGATION TO IMPROVE THE LOW-SPEED LONGITUDINAL STABILITY AT HIGH LIFT OF A SUPERSONIC TRANSPORT WITH VARIABLE-SWEEP WINGS

by Anthony M. Cook and Dale G. Jones

Ames Research Center
Moffett Field, Calif.

NATIONAL AERONAUTICS AND SPACE ADMINISTRATION • WASHINGTON, D. C. • JANUARY 1969

NASA TN D-5005

LARGE-SCALE WIND-TUNNEL INVESTIGATION TO IMPROVE THE LOW-SPEED LONGITUDINAL STABILITY AT HIGH LIFT OF A SUPERSONIC TRANSPORT WITH VARIABLE-SWEEP WINGS

By Anthony M. Cook and Dale G. Jones

Ames Research Center
Moffett Field, Calif.

NATIONAL AERONAUTICS AND SPACE ADMINISTRATION

For sale by the Clearinghouse for Federal Scientific and Technical Information
Springfield, Virginia 22151 – CFSTI price $3.00

LARGE-SCALE WIND-TUNNEL INVESTIGATION TO IMPROVE THE LOW-SPEED LONGITUDINAL STABILITY AT HIGH LIFT OF A SUPERSONIC TRANSPORT WITH VARIABLE-SWEEP WINGS

By Anthony M. Cook and Dale G. Jones

Ames Research Center

SUMMARY

An investigation has been made in the Ames 40- by 80-Foot Wind Tunnel to develop techniques to improve the longitudinal stability for a supersonic transport. The model had a wing pivot outboard of the fuselage, a high aspect-ratio movable wing panel, and a highly swept, fixed, inboard wing portion (strake). Special efforts were made to minimize the adverse effects of the vortex flow from the highly swept strake leading edge. Flow control devices tested on the strake included increased leading-edge radius, leading-edge (Krueger-type) flaps, and upper-surface vortex generators. Fences on both strake and movable wing panel were also tested.

The results show the basic model with a sharp strake leading edge to have pitch-up at an angle of attack as low as 5°. The use of a larger strake leading-edge radius together with a strake leading-edge flap and a wing fence produced essentially linear pitching-moment characteristics to 18° angle of attack, with a stable break at stall. A combination of vortex generators on the strake upper surface, and a wing fence outboard of the pivot also produced acceptable pitching-moment characteristics.

The results are presented as longitudinal aerodynamic force and moment data obtained at various angles of attack. The majority of the investigation was made at a free-stream dynamic pressure of 22 pounds per square foot, corresponding to a Reynolds number of 19 million, based upon the mean aerodynamic chord of the fully swept wing.

INTRODUCTION

Previous investigations of the variable-sweep concept have shown the advantages of locating the wing pivot outboard from the fuselage (ref. 1). With this pivot location, a highly swept inboard portion of the wing remains fixed. The inboard portion of the wing, or strake, is located ahead of the center of gravity and causes a nonlinear variation of pitching moment with angle of attack (refs. 2 and 3). This instability is considered to be largely attributable to the effect of the vortex shed from the strake leading edge. The vortex apparently induces separation over the movable wing panel in the area of the panel-strake juncture. This separation limits both maximum lift and the contribution of trailing-edge flaps to maximum lift.

The object of this investigation was to study techniques for controlling or delaying the formation of the strake vortex. Flow control devices tested on the strake included leading-edge radius, leading-edge (Krueger type) flaps, and upper-surface vortex generators. Fences on both strake and movable wing panel were studied. Also assessed was the effectiveness of such high lift devices as single-slotted, double-slotted, and boundary-layer-control flaps.

NOMENCLATURE

b	wing span, ft
BLC	boundary-layer control
c	chord
$\bar{c}$	mean aerodynamic chord of fully swept wing, $\frac{2}{S}\int_0^{b/2} c^2\,dy$, ft
C_D	drag coefficient, $\frac{\text{drag}}{qS}$
C_L	lift coefficient, $\frac{\text{lift}}{qS}$
C_m	pitching-moment coefficient, $\frac{\text{pitching moment}}{qS\bar{c}}$
C_μ	momentum coefficient, $\frac{M_j V_j}{qS}$
g	minimum gap of a high-lift device, percent of chord
i_T	horizontal-tail incidence (positive, trailing edge down), deg
K_1	constant-chord leading-edge (Krueger) flap on strake
K_2	tapered-chord leading-edge (Krueger) flap on strake
ℓ	length, ft
ℓ_T	tail length, measured from 40 percent $\bar{c}$ to 25 percent of the tail mean aerodynamic chord, ft
M_j	mass-flow rate of the boundary-layer-control system, slugs/sec
N	strake leading-edge notch

q	free-stream dynamic pressure, lb/ft^2
r	radius
R-1	sharp strake leading edge
R-2	tapered radius strake leading edge
R-3	constant (large) radius strake leading edge
S	wing area of the fully swept wing, ft^2
SF	strake fence
VG	vortex generators
V_j	velocity of the boundary-layer-control jet, ft/sec
$\overline{V}_T$	tail volume coefficient, $\frac{S_T}{S} \times \frac{\ell_T}{\bar{c}}$
WCP	wing chord plane (corresponding to the flat, lower surface of the movable outer wing portion)
WF	wing fence
x	streamwise distance along airfoil chord, ft
y	spanwise distance perpendicular to the plane of symmetry, ft
z	perpendicular distance from wing chord plane, ft
α	angle of attack of the wing chord plane, deg
δ	angle of deflection of a control surface, downward from the WCP, measured normal to the hinge line, deg
η	wing semispan station, $\frac{2y}{b}$
λ	wing taper ratio
Λ	angle of sweepback of movable wing leading edge, deg

Subscripts

F	flap
FBLC	boundary-layer-control flap

FDS	double-slotted flap
FSS	single-slotted flap
ℓ	lower surface
LE	leading edge
s	slat
T	tail
u	upper surface
w	wing

MODEL

The model was an unpowered, supersonic transport configuration with a low wing (figs. 1 and 2(a)). The wing leading-edge sweepback angles were adjustable from 18° to 75°. The fuselage was of circular cross section, with a fineness ratio of 16.5. The wing pivots were located at the 56.5 percent longitudinal fuselage station ($0.46\bar{c}$), and 33.8 percent of the fully swept semispan outboard from the model centerline. (Model dimensions given as percentages of $\bar{c}$ refer to the mean aerodynamic chord of the fully swept, total wing planform.) Model geometry is given in table I.

Wing

Inboard fixed portion (strake).- Streamwise strake airfoil sections are located and defined by coordinates in figures 2(b) and 2(c). Strake sections were twisted and contoured to provide a positive 1° incidence at the fuselage and 0° incidence outboard at the wing pivot. The resulting airfoil provided a continuous, smooth fairing into the fully swept outer wing panel. Strake leading-edge sweepback angle was fixed at 75°.

Outboard movable portion.- The leading-edge sweepback of the movable panel was adjustable from 18° to 75°. The outboard portion had no twist, incidence, or dihedral. The variation in geometry with sweepback angle is given in table I. The airfoil section of the movable wing had a flat lower surface and the thickness distribution of a NACA 65A006 airfoil section (streamwise at 25° sweep). (See figs. 2(b) and 2(c) for wing airfoil sections and coordinates.)

Horizontal Tail

The airfoil section of the aspect ratio 2.6 horizontal tail consisted of a symmetrical 3-percent circular-arc section with sharp leading and trailing edges. The tail was fuselage mounted as shown in figure 2(a), and had no dihedral. Tail incidence was varied from 0° to -15°. See table I for additional tail geometry.

High Lift Devices

Wing trailing-edge flaps.- The movable portion of the wing was adapted for installation of single-slotted, double-slotted, and boundary-layer-control (BLC) flaps. Flap sections extended spanwise from the wing-strake juncture to 65 percent of the semispan (18° sweep). The configurations and coordinates of the three flap systems are given in figures 2(d), 2(e), and 2(f). The single-slotted flap was 0.21 c_w long (parallel to the plane of symmetry at 25° sweep), was deflected along a hinge line at 0.73 c_w, and had a flap gap of 0.01 c_w. The double-slotted flap was 0.24 c_w long, was deflected at a hinge line of 0.77 c_w, and was adjustable for deflections to 60° from the wing chord plane. The boundary-layer-control flap and auxiliary equipment was capable of momentum coefficients (C_μ) up to 0.048 through a 0.027-inch spanwise nozzle on the flap upper radius at the 0.70 hinge line. The BLC flap was deflectable to 60°.

Wing leading-edge slats.- The movable wing was equipped with full-span leading-edge slats. Slat chord was 0.15 c_w and gap was 0.02 c_w. The slats were adjustable for deflections to 35° downward from the wing chord plane. The slats are defined further in figure 2(g).

Flow Control Devices

Strake leading edges.- The strake was adapted for the installation of three different leading edges; one of sharp contour, one of tapering radius and one of large, constant radius. The sharp leading edge (R-1) is defined in figure 2(b) and is the basic strake airfoil section leading edge. The tapered radius leading edge (R-2) was a half-cone varying linearly from a radius of 0.015 $\bar{c}$ at the fuselage-strake juncture to 0.004 $\bar{c}$ at the wing strake juncture (fig. 1(a)). The large constant-radius leading edge (R-3) was a half-cylinder with a radius of 0.023 $\bar{c}$ (fig. 1(c)). The half-cone and the half-cylinder were installed tangent to the strake upper surface and faired smoothly into the strake lower surface as shown in figure 2(b).

Strake leading-edge flaps.- Two shapes of slotted, Krueger-type flaps were tested on the strake leading edge. One (K_1) had a constant chord of 0.034 $\bar{c}$ (perpendicular to the leading edge). The other (K_2) had a non-linearly tapering chord from 0.030 $\bar{c}$ inboard to 0.080 $\bar{c}$ outboard at the wing-strake juncture. Both flaps were deflected 70° downward from the wing-chord plane, and the flap gap was 0.0047 $\bar{c}$ unless otherwise indicated. Details of the geometry and installation are given in figure 2(g).

Strake vortex generators.- Two thin-plate, triangular vortex generators were installed on the strake upper surface, normal to the wing chord plane and near the strake leading edge. The vortex generators were 0.129 $\bar{c}$ long and 0.044 $\bar{c}$ high and were positioned as shown in figure 2(h).

Fences.- Two fences were available for separate use on the movable wing panel and strake upper surfaces. They were both 0.045 $\bar{c}$ high and were mounted streamwise and normal to the wing chord plane. (See fig. 2(h).)

Notch.- A streamwise notch was cut in the strake leading edge, just inboard of the wing-strake juncture (see fig. 2(h)). The notch was 0.015 $\bar{c}$ spanwise and 0.076 $\bar{c}$ in chordwise length.

TESTING AND PROCEDURE

Six-component force and moment data were obtained for angles of attack from -4° to +30°, and wing sweepback angles of 18°, 29°, and 40°. Free-stream dynamic pressure for the majority of testing was 22.0 pounds per square foot. This dynamic pressure corresponds to a Reynolds number of 19 million, based on the fully swept mean aerodynamic chord. (The effect of Reynolds number variation is shown in fig. 10.)

The majority of tests was made with 30° single-slotted flaps, 35° wing slats, -5° tail incidence, and various combinations of flow control devices. Three strake leading edges and two Krueger-type strake leading-edge flaps were tested to evaluate the effects of leading-edge geometry on vortex formation and pitching-moment characteristics. Other devices tested to determine their influence on the strake vortex included strake upper-surface vortex generators, fences, and a leading-edge notch. The vortex generators were installed on the strake upper surface to create vortices intended to counteract the strake vortex. Upper surface wing and strake fences were installed to contain the strake vortex and prevent it from moving outboard along the wing. A notch was cut in the strake leading edge to disrupt vortex formation.

High-lift devices on the wing were tested in various combinations with the flow control devices to determine the effects of flap geometry, flap deflection, and BLC momentum coefficient. The intent of this part of the investigation was to maximize the total lift while maintaining longitudinal stability.

REDUCTION OF DATA

Corrections

Standard corrections for wind-tunnel wall effects were applied to the lift and drag data. The corrections accounted for variations in span due to wing sweep, and are as follows:

$$\alpha = \alpha_{uncorrected} + \Delta\alpha$$

$$C_D = C_{D_{uncorrected}} + \Delta C_D$$

Wing sweep	18°	29°	40°
$\frac{\Delta\alpha}{C_L}$	0.90	0.92	0.94
$\frac{\Delta C_D}{C_L{}^2}$	0.0159	0.0161	0.0164

In addition, drag and pitching-moment data were corrected to account for wind forces on the exposed portions of the model support struts. These additive corrections were

$$\Delta C_D = -0.0076$$

$$\Delta C_m = +0.0040$$

Reference Dimensions

The computation of force and moment coefficients was based upon the dimensions corresponding to the fully swept-wing configuration, as follows:

$$S = 494.8 \text{ ft}^2$$

$$\bar{c} = 22.0 \text{ ft}$$

$$b = 26.6 \text{ ft}$$

The moment center was located at the wing pivot axis, 46 percent of the mean aerodynamic chord, and 0.034 $\bar{c}$ above the wing chord plane.

The momentum coefficient (C_μ) of the boundary-layer-control system was derived from total- and static-pressure readings in the duct system. The jet velocity and mass flow rate necessary for the derivation were calculated from the pressure readings assuming isentropic flow.

RESULTS

The results are arranged in groups by wing sweepback angle as follows:

Λ	Figures
18°	3-11
29°	12-16
40°	17-19

The effects of geometry, high-lift devices, and pitch control on the longitudinal aerodynamic characteristics are presented for each group. Comparisons of wing sweep are shown in figures 20 through 22. A complete index to the data figures is given in table II.

DISCUSSION

Longitudinal Stability

Variable-sweep wing configurations with fixed, highly swept inboard leading edges generally have unstable pitching-moment characteristics at high angles of attack. This is largely due to the vortex caused by spanwise pressure gradients generated along the highly swept inboard leading edge. At high angles of attack, upwash from the vortex causes separation of the flow over the outboard wing panel while strake lift continues to increase. The resulting forward shift in aerodynamic center produces the pitching-moment nonlinearity that becomes unstable.

Flow control devices.- Many devices were tested in an effort to weaken or counteract the strake vortex.

The effect of larger radius on the strake leading edge was to delay formation of the strake vortex and prolong pitching-moment linearity. As shown in figure 3, the upper limit of α for pitching-moment stability increased from 5° for the sharp strake leading edge to 11° for the large constant-radius leading edge.

The strake leading-edge notch was apparently ineffective in disrupting vortex formation, and there was negligible change in the pitching-moment characteristics due to the notch, as shown in figure 4.

The wing fence was slightly more effective than the strake fence in containing the strake vortex and preventing its flow outboard over the root of the movable wing. A comparison of the effects of the two fences, referenced to the case with no fences, is given in figure 5(b). The fence encouraged a stable break in the pitching-moment curve at the point of stall of the movable wing.

The constant-chord leading-edge flap (K_1), with the tapered radius leading edge (R-2) was effective in improving pitching-moment linearity, as shown in figure 6(a). This combination produced a negative C_{m_0} shift of 0.014 and resulted in a stable break at stall.

The combination of the constant-chord leading-edge flap (K_1) on the strake, and the wing fence, with the tapered radius leading edge (R-2) (fig. 6(d)), produced an essentially linear pitching-moment curve to 18° angle of attack and C_L of 1.45, beyond which the moment curve broke stable. This combination of flow control devices produced the most desirable pitching-moment characteristics of all the combinations tested. The improved stability attributed to the wing fence, in combination with the strake leading-edge flap, is readily seen in figure 6(d).

It should be pointed out that the vortex generators, combined with the wing fence, improved the pitching-moment linearity and stall characteristics better than the constant-chord strake leading-edge flap alone. This can be seen by comparing figures 6(d) and 6(a).

Longitudinal Control

The effects of horizontal-tail incidence on longitudinal characteristics are depicted in figures 11, 16, and 18. Control power (dC_m/di_t) was an essentially constant -0.0130 per degree throughout the angle-of-attack range tested.

High Lift

Trailing-edge flaps.- The longitudinal characteristics of single-slotted, double-slotted, and blowing boundary-layer-control flaps are presented in figure 8. The 50° BLC flap, at $C_\mu = 0.047$ (fig. 8(a)), had a 0.65 greater lift increment at 0° angle of attack than the 30° single-slotted flap, and 0.45 greater than the 50° double-slotted flap. (Single-slotted flap deflections greater than 30° yield little increase in effectiveness, as shown in fig. 7.) However, the advantages of the BLC flap are negated by the vortex, since $C_{L_{max}}$ is not increased and the pitch-up at $C_{L_{max}}$ is more pronounced. The stall characteristics with all flap systems were less severe and pitching-moment linearity was improved when the constant-chord leading-edge flap (K_1) on the strake was replaced with the combination of vortex generators and wing fence (see fig. 8(b)). The effects of momentum coefficient and deflection angle for the BLC flap are shown in figure 9. An increase in flap deflection at constant C_μ yields increased lift at $\alpha = 0°$, but no increase in $C_{L_{max}}$ for deflections greater than 40°.

Leading-edge slats.- The effects of leading-edge slats on the movable wing panel at 40° sweep are depicted in figure 19. As expected, a slotted slat deflected 35° delays the stall of the outer wing panel and improves the lift/drag ratio above 8° angle of attack. Improved pitching-moment linearity can be see to result from the delay in outer wing panel stall.

Effect of Wing Sweepback

The aft movement of the aerodynamic center with increasing wing sweepback angle is evident in the data of figures 20 through 22. A change in wing sweepback angle from 18° to 29° (fig. 20) caused an increase in static margin from 8- to 14-percent $\bar{c}$. The lift-curve slope was reduced 27 percent, from 0.11 to 0.08/deg (fig. 21). For this wing-sweep change the aspect ratio changed from 9.0 to 7.6.

SUMMARY OF RESULTS

An investigation has been made in the Ames 40- by 80-Foot Wind Tunnel to improve the low-speed longitudinal stability at high lift for a supersonic transport with wings of variable sweep. The major results of this investigation are summarized as follows:

1. The basic model with a sharp strake leading edge had pitch-up at 5° angle of attack.

2. The relative effectiveness of flow control devices in the order of improvement to pitching moment is as follows:

   (a) A strake leading edge of large radius extended pitching-moment stability to 11° angle of attack and reduced the severity of the pitch-up.

   (b) The combination of a strake leading edge with a tapered radius, vortex generators on the strake upper surface, and a wing fence outboard of the pivot was effective in linearizing the pitching moment to 15° angle of attack.

   (c) A strake leading-edge flap, a tapered radius strake leading-edge, and a wing fence were the most effective combination, providing an essentially linear pitching moment to 18° angle of attack, with a stable break at stall.

3. For all the strake leading-edge configurations, increased trailing-edge flap effectiveness did not increase $C_{L_{max}}$.

Ames Research Center
National Aeronautics and Space Administration
Moffett Field, Calif., 94035,
720-01-00-01-00-21

REFERENCES

1. Spencer, Bernard, Jr.: Stability and Control Characteristics at Low Subsonic Speeds of an Airplane Configuration Having Two Types of Variable-Sweep Wings. NASA TM X-303, 1960.

2. Cook, Anthony M.; Greif, Richard K.; Aoyagi, Kiyoshi: Large-Scale Wind-Tunnel Investigation of the Low-Speed Aerodynamic Characteristics of a Supersonic Transport Model Having Variable-Sweep Wings. NASA TN D-2824, 1965.

3. Lockwood, Vernard E.: Low-Speed Wind-Tunnel Studies Relating to Pitch-Up on a Supersonic Transport Model With a High-Aspect-Ratio Variable-Sweep Wing. NASA TN D-3542, 1966.

TABLE I.- AERODYNAMIC REFERENCE DIMENSIONS

Wing:	
Area (fully swept, 75°), ft^2	494.80
$\bar{c}$ (fully swept, 75°), ft	22.00
Span	
18° sweep, ft	55.80
29° sweep, ft	51.50
40° sweep, ft	48.40
75° sweep, ft	26.60
Aspect ratio	
18° sweep	9.00
29° sweep	7.60
40° sweep	6.60
75° sweep	1.40
Fuselage:	
Length, ft	66.56
Maximum width, ft	4.00
Horizontal tail:	
Area, exposed, ft^2	100.00
Span, ft	18.35
Aspect ratio	2.62
Taper ratio	0.20
Tail length, ℓ_T, ft	24.40
$\bar{c}_T$, ft	7.10
Tail volume coefficient	0.225

TABLE II.- INDEX TO DATA FIGURES

18° Wing sweep:	Strake L.E.	Figure
Effects of vortex flow control devices		
Strake leading edge	R-1,2,3	3
L.E. notch, strake fence, vortex generators	R-1	4
Wing fence, strake fence, vortex generators	R-3	5
Strake L.E. flaps, fences, vortex generators.	R-2	6
Effects of wing trailing-edge flaps		
Single-slotted, with and without fence and vortex generators.	R-3	7
Single-slotted, double-slotted, and BLC flaps.	R-2	8
BLC flap deflection and momentum coefficient.	R-2	9
Miscellaneous effects		
Reynolds number variation	R-3	10
Horizontal-tail incidence	R-3	11
29° Wing sweep:		
Effects of vortex flow control devices		
Strake leading edge	R-2,3	12
Vortex generators and strake L.E. flap.	R-2	13
Wing trailing-edge flaps		
Single-slotted flap deflection.	R-3	14
Single-slotted and double-slotted flaps	R-2	15
Horizontal-tail effects	R-3	16
40° Wing sweep:		
Flow control devices.	R-3	17
Horizontal tail on and off.	R-3	18
Wing leading-edge slats	R-3	19
Variable wing-sweep effects:		
18° and 29° sweep (N+SF).	R-1	20
18° and 29° sweep (VG).	R-3	21
29° and 40° sweep (clean, tail off)	R-3	22

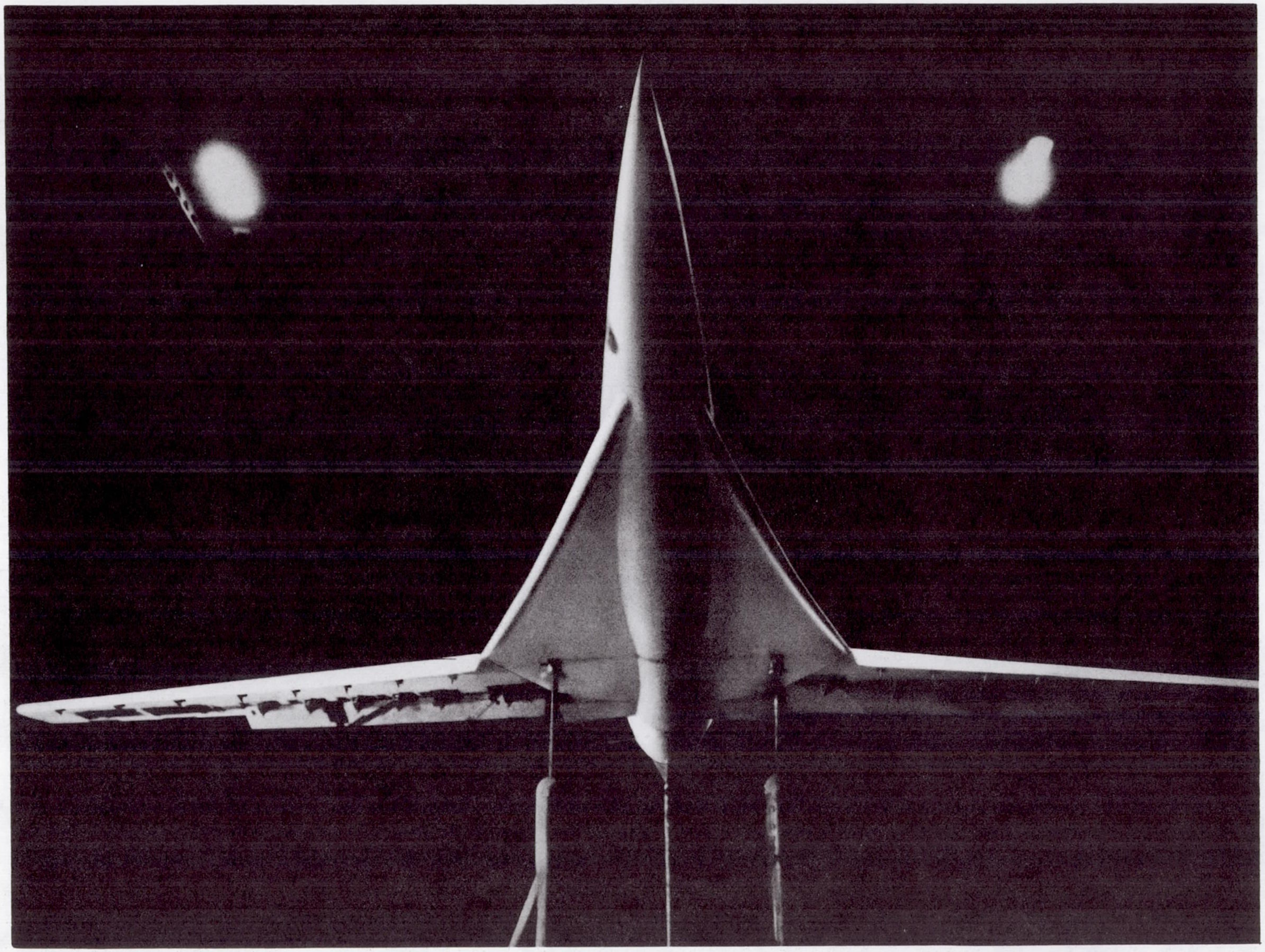

A-38991.1

(a) Front view showing strake with tapered leading-edge radius.

Figure 1.- Photographs of the model mounted in the 40- by 80-foot wind tunnel.

A-36184

(b) Three-quarter front view showing constant-chord strake leading-edge flap.

Figure 1.- Continued.

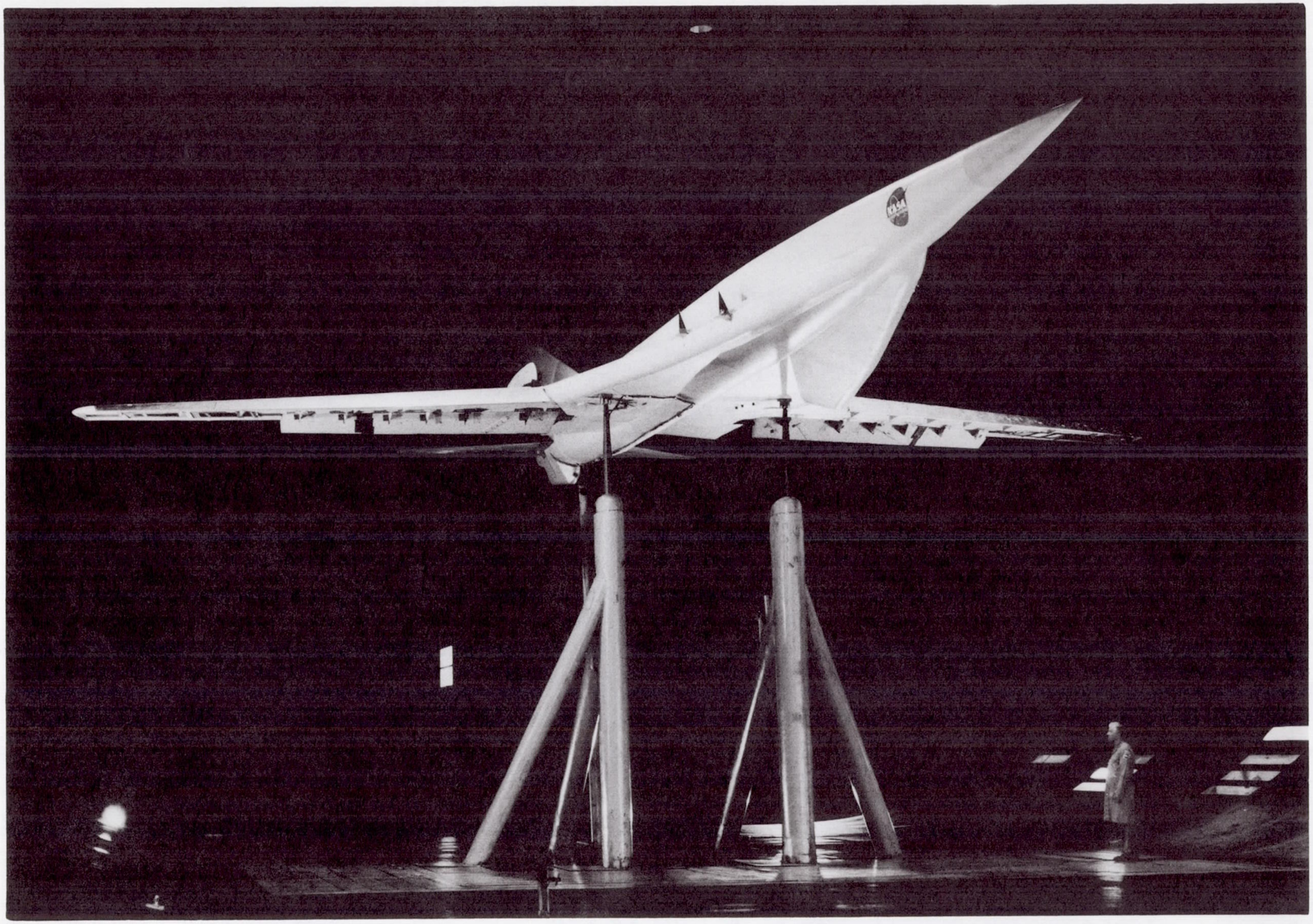

A-33012

(c) Three-quarter front view showing strake vortex generators and wing fence.

Figure 1.- Concluded.

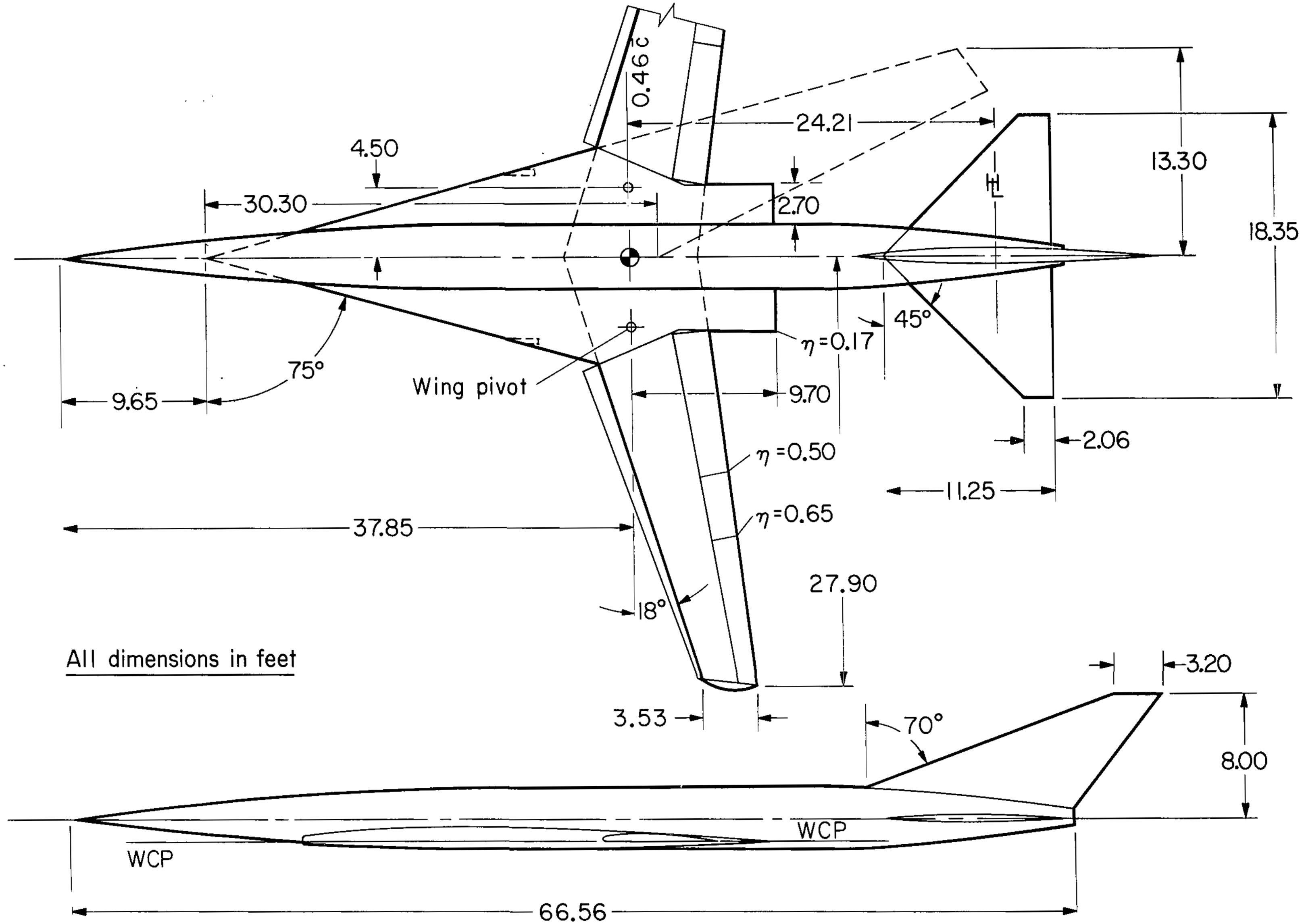

(a) Complete model.

Figure 2.- Geometric details of the model.

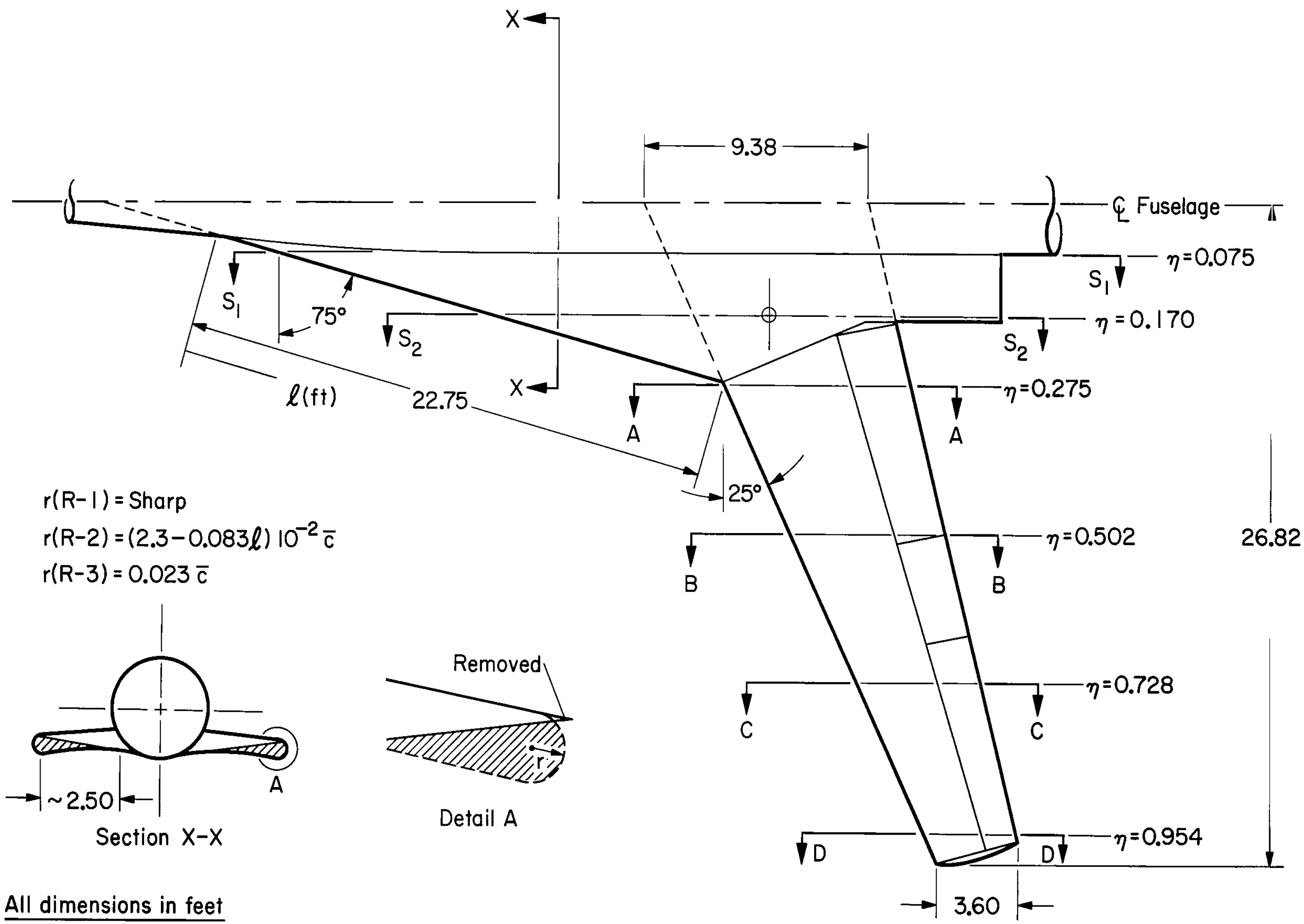

(b) Strake and wing section locations - see figure 2(c) for coordinates.

Figure 2.- Continued.

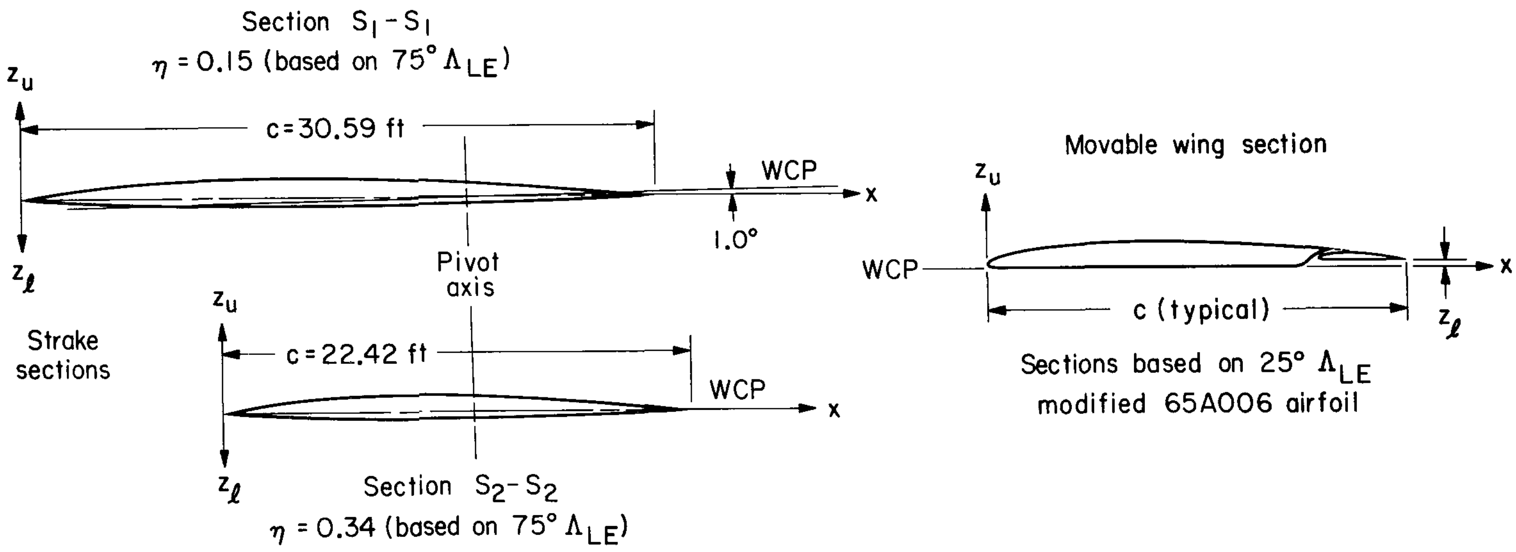

x/c	Section S_1-S_1		Section S_2-S_2	
	z_u/c	z_ℓ/c	z_u/c	z_ℓ/c
0	0	0	0	0
.0050	.0007	.0002	.0026	.0020
.0075	.0011	.0003	.0030	.0022
.0125	.0018	.0005	.0038	.0025
.0250	.0035	.0010	.0058	.0032
.0500	.0070	.0019	.0095	.0045
.0750	.0102	.0029	.0129	.0058
.1000	.0132	.0038	.0160	.0069
.1500	.0183	.0054	.0217	.0091
.2000	.0222	.0068	.0263	.0109
.2500	.0253	.0080	.0300	.0125
.3000	.0275	.0091	.0327	.0139
.3500	.0290	.0100	.0345	.0150
.4000	.0297	.0108	.0351	.0155
.4500	.0296	.0114	.0345	.0151
.5000	.0288	.0118	.0329	.0140
.5500	.0273	.0121	.0306	.0125
.6000	.0251	.0123	.0279	.0109
.6500	.0223	.0123	.0249	.0092
.7000	.0193	.0120	.0217	.0076
.7500	.0161	.0113	.0183	.0060
.8000	.0127	.0100	.0148	.0046
.8500	.0094	.0082	.0112	.0033
.9000	.0061	.0058	.0076	.0010
1.0000	0	0	0	0

x/c	Section A-A(η=0.275)		Section B-B(η=0.502)		Section C-C(η=0.728)		Section D-D(η=0.954)	
	z_u/c	z_ℓ/c	z_u/c	z_ℓ/c	z_u/c	z_ℓ/c	z_u/c	z_ℓ/c
0	0.00748	0	0.00727	0	0.00694	0	0.00642	0
.0073	.01543		.01498		.01395		.01307	
.0086	.01598		.01533		.01492		.01398	
.0130	.01756		.01672		.01650		.01552	
.0260	.02159		.02044		.02029		.01952	
.0500	.02741		.02667		.02630		.02488	
.0780	.03334		.03315		.03270		.03106	
.1000	.03770		.03729		.03621		.03460	
.1500	.04500		.04479		.04330		.04088	
.2000	.05070		.05052		.04850		.04622	
.2500	.05538		.05500		.05260		.05031	
.3000	.05927		.05844		.05655		.05382	
.3500	.06300		.06083		.05890		.05465	
.4000	.06422		.06219		.06000		.05520	
.4500	.06443		.06240		.05930		.05359	
.5000	.06342		.06167		.05725		.05051	
.5500	.06106		.05969		.05440		.04812	
.6000	.05820		.05625		.05125		.04540	
.6500	.05502		.05208		.04740		.04202	0.00506
.7000	.05113		.04688		.04320	0.00578	.03830	.00506
.7500	.04550	0.00622	.04104	0.00604	.03770	.00578	.03388	.00506
.8000	.03872	.00622	.03458	.00604	.03280	.00578	.02950	.00506
.8500	.03218	.00622	.02750	.00604	.02720	.00578	.02551	.00506
.9000	.02499	.00622	.02052	.00604	.02071	.00578	.01906	.00506
.9500	.01640	.00622	.01333	.00604	.01365	.00578	.01289	.00506
1.0000	.00622	.00622	.00604	.00604	.00578	.00578	.00506	.00506

(c) Coordinates of strake and wing airfoil sections of figure 2(b).

Figure 2.- Continued.

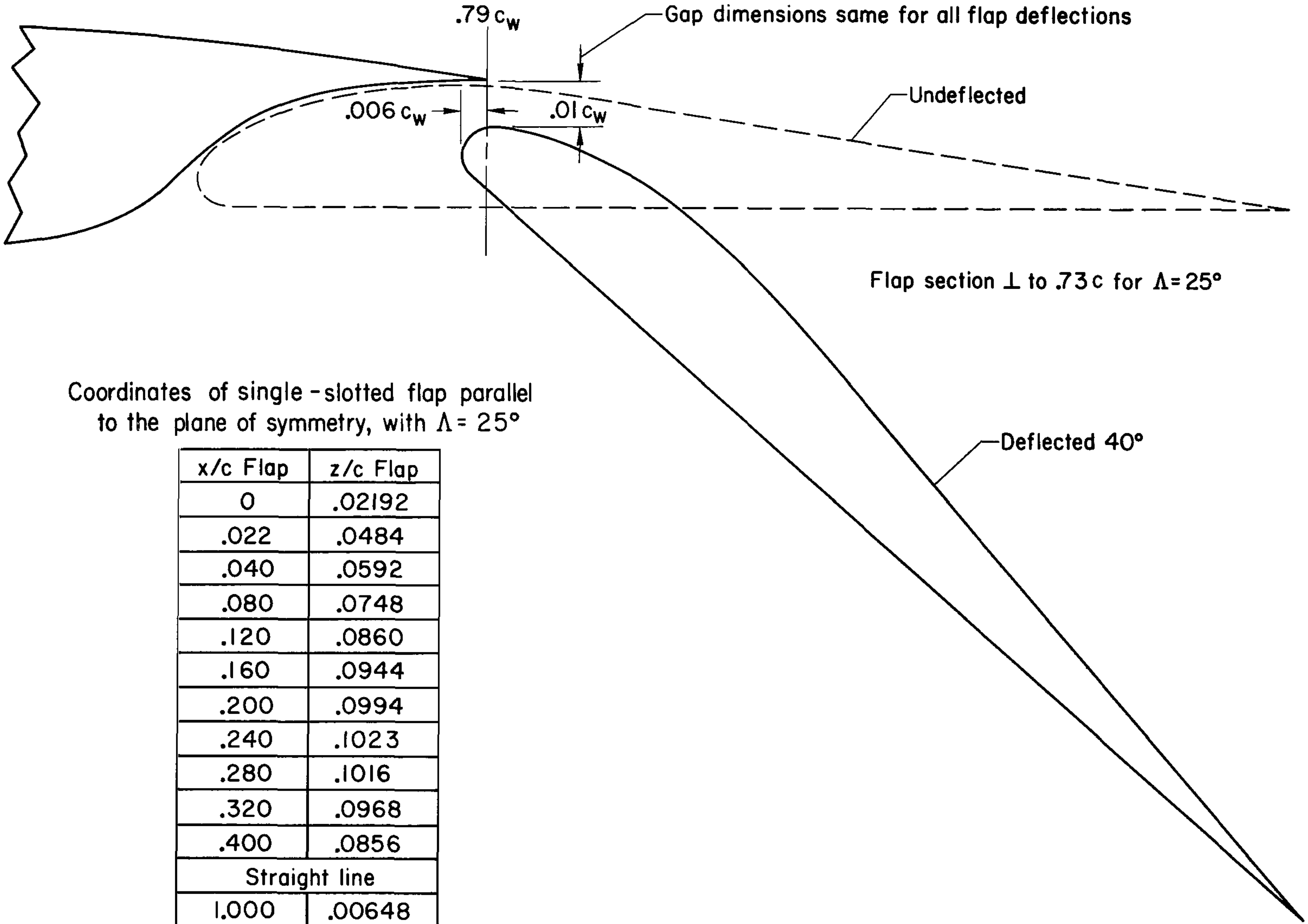

Coordinates of single-slotted flap parallel to the plane of symmetry, with Λ = 25°

x/c Flap	z/c Flap
0	.02192
.022	.0484
.040	.0592
.080	.0748
.120	.0860
.160	.0944
.200	.0994
.240	.1023
.280	.1016
.320	.0968
.400	.0856
Straight line	
1.000	.00648
L.E. radius = .02192	

(d) Details of the single-slotted flap.

Figure 2.- Continued.

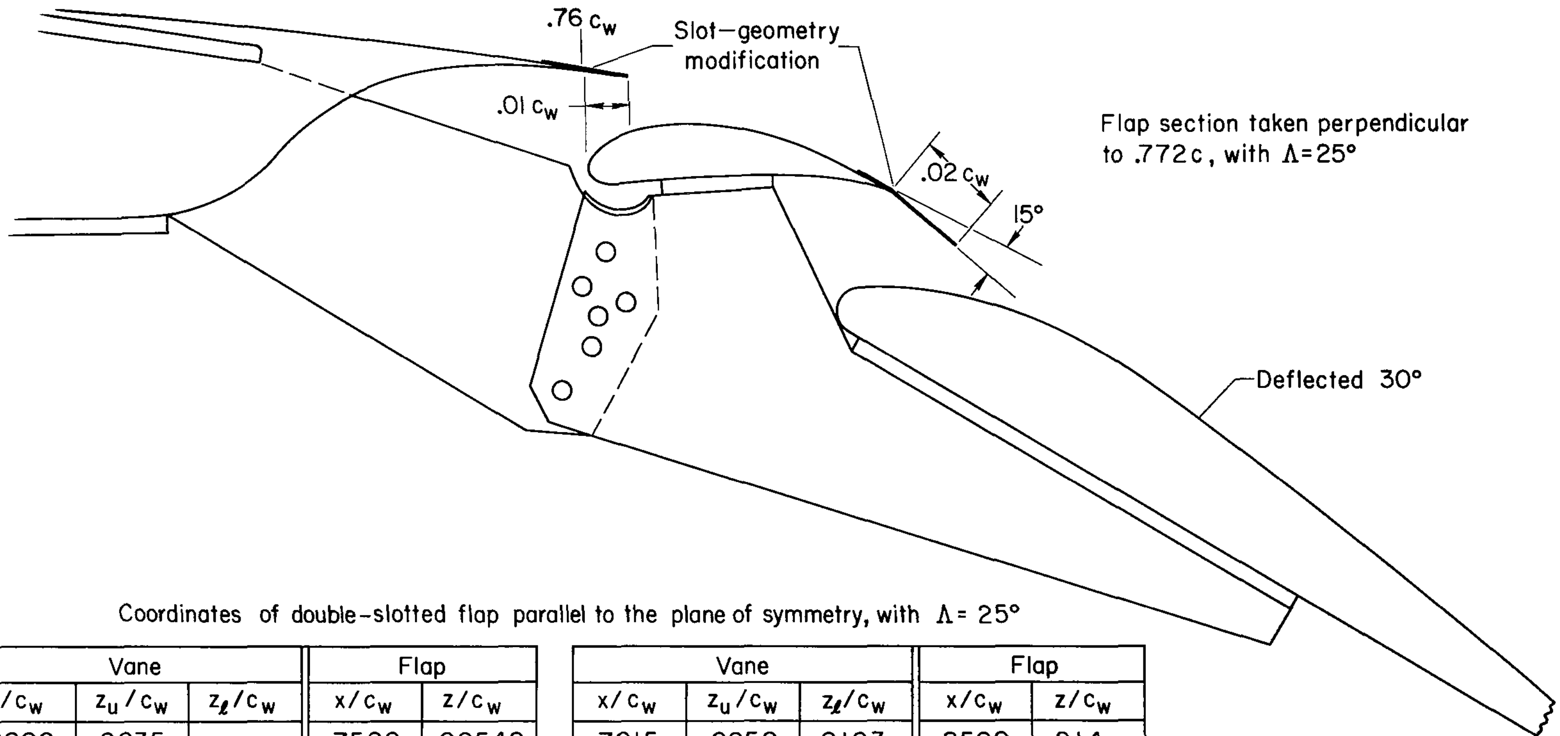

Coordinates of double-slotted flap parallel to the plane of symmetry, with $\Lambda = 25°$

Vane			Flap	
x/c_w	z_u/c_w	z_l/c_w	x/c_w	z/c_w
.6800	.0035	—	.7500	.00548
.6803	.0047	.0022	.7555	.0121
.6807	.0061	.0015	.7600	.0148
.6816	.0084	.0007	.7700	.0187
.6835	.0116	0	.7800	.0215
.6853	.0140	.0004	.7900	.0236
.6872	.0156	.0010	.8000	.0249
.6888	.0172	.0018	.8100	.0256
.6921	.0197	.0037	.8200	.0254
.6953	.0217	.0059	.8300	.0242

Vane			Flap	
x/c_w	z_u/c_w	z_l/c_w	x/c_w	z/c_w
.7015	.0250	.0103	.8500	.214
.7077	.0277	.0145	Straight line	
.7141	.0299	.0186	1.0000	.0016
.7207	.0312	.0225		
.7273	.0322	.0261	L.E. radius=.00548	
.7342	.0329	.0290		
.7414	.0334	.0314		
.7450	.0335	.0325		
.7486	.0332	.0332		

(e) Details of the double-slotted flap.

Figure 2.- Continued.

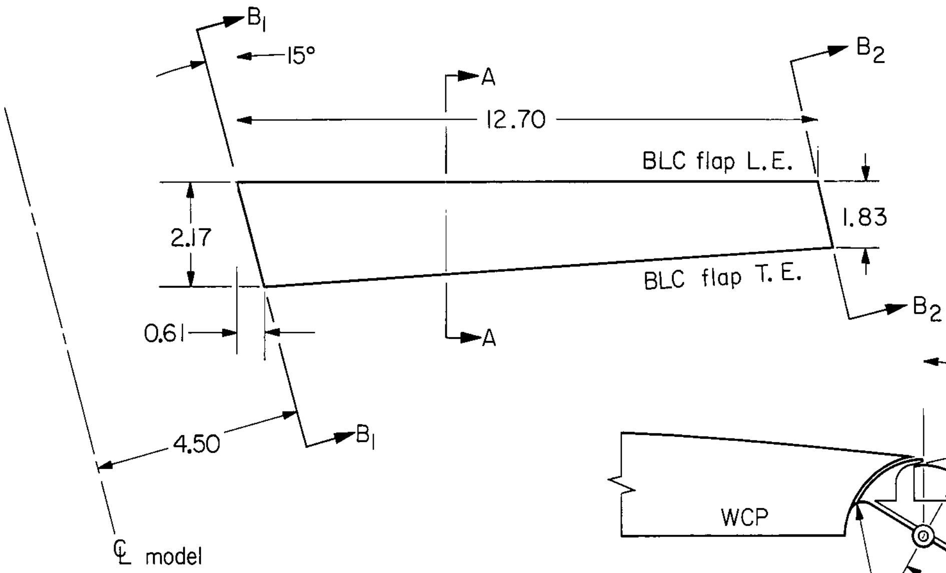

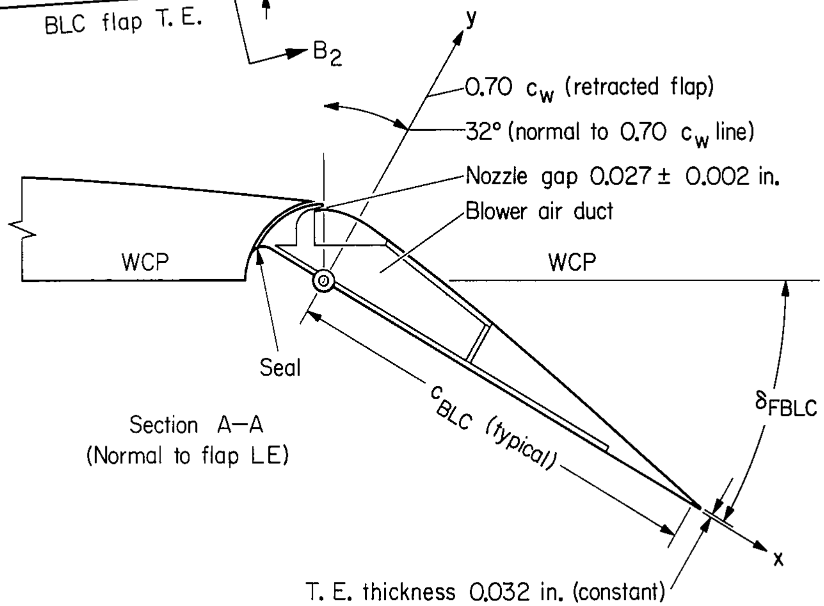

Coordinates of BLC flap parallel to the plane of symmetry, with Λ = 25°

Streamwise sections B_1-B_1, B_2-B_2		
x/c_w	x/c_{flap}	z/c_{flap}
0.7000	0	0.1390
0.7500	0.1667	0.1180
0.8000	0.3333	0.0955
0.8500	0.5000	0.0720
0.9000	0.6667	0.0480
0.9500	0.8333	0.0245

All dimensions in feet unless otherwise noted

(f) Details of the boundary-layer-control flap.

Figure 2.- Continued.

Strake leading edge flap deflections

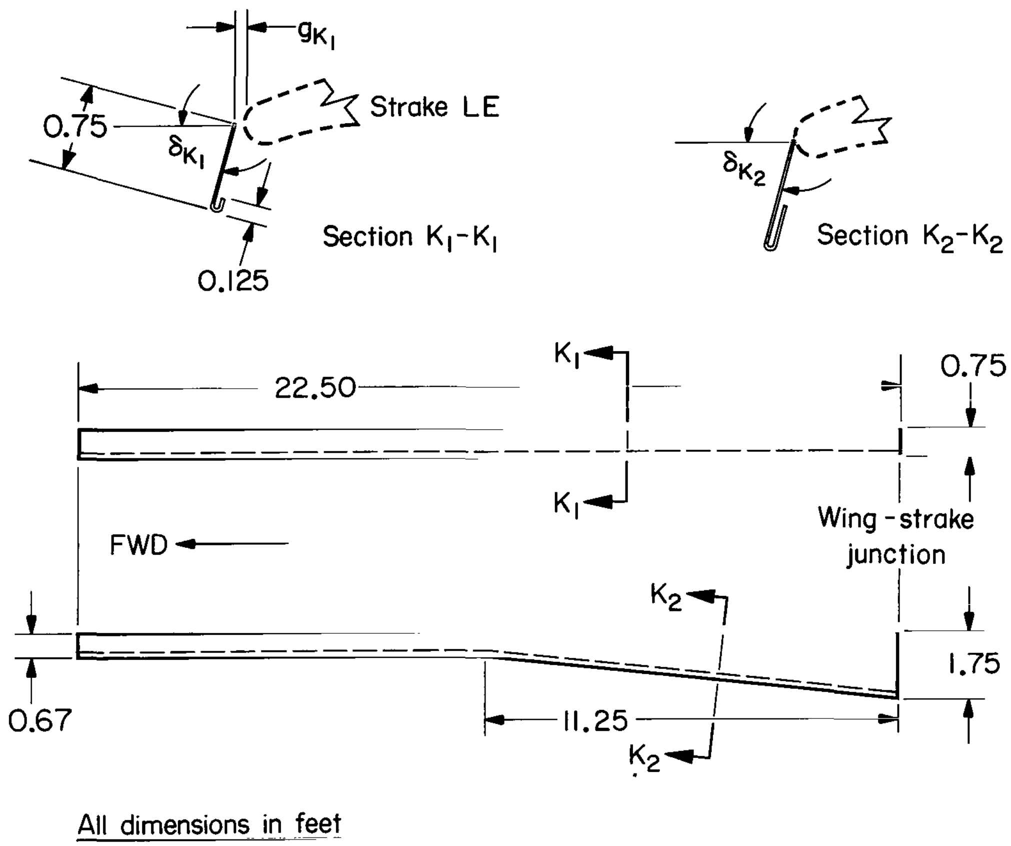

Wing leading edge slat deflections

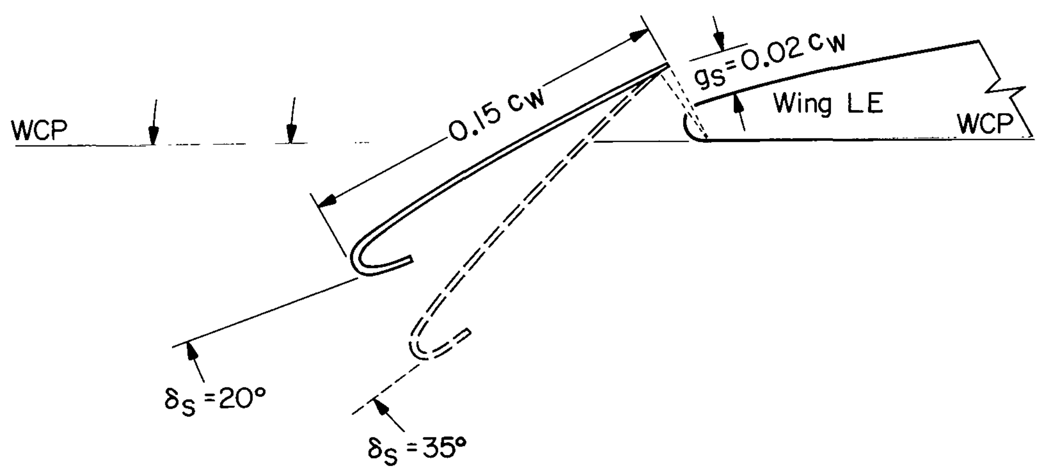

(g) Details of strake leading-edge flaps and wing leading-edge slats.

Figure 2.- Continued.

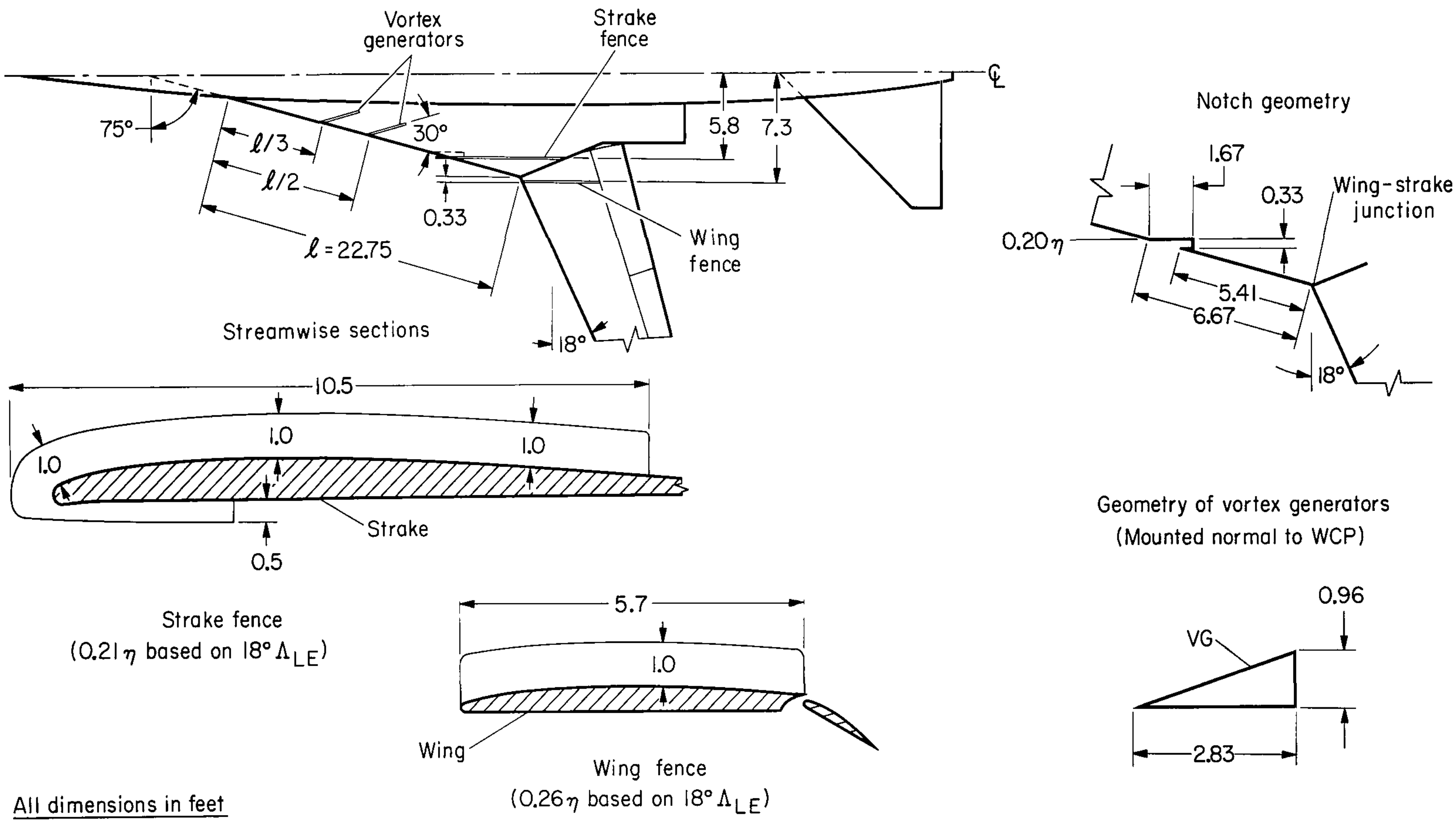

(h) Details of strake vortex generators, notch, and fences.

Figure 2.- Concluded.

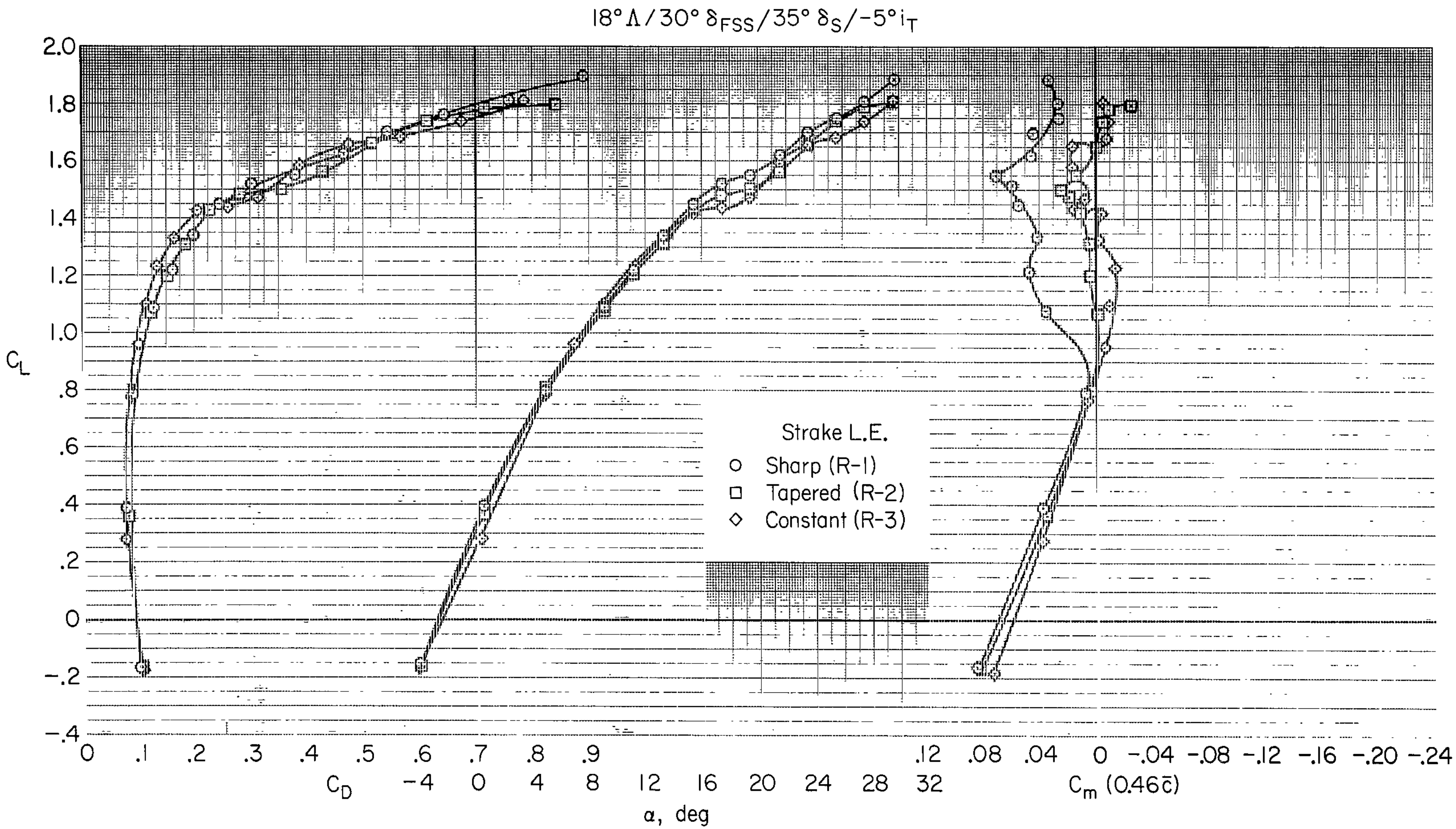

Figure 3.- Effect of strake leading-edge radius on the longitudinal characteristics with 18° wing sweep.

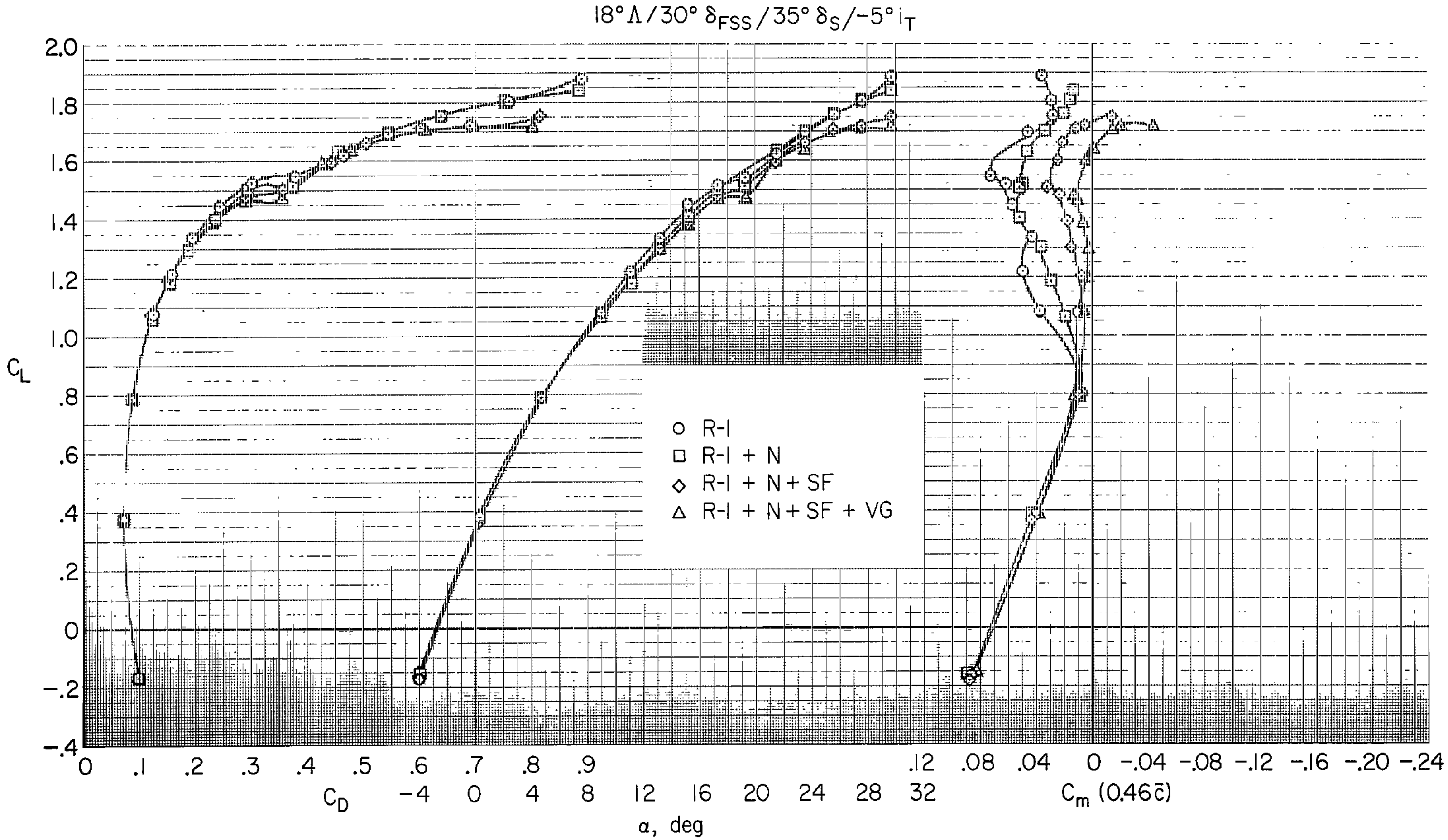

Figure 4.- Aerodynamic effects of strake leading-edge notch, strake fence, and vortex generators with the sharp strake leading edge; 18° wing sweep.

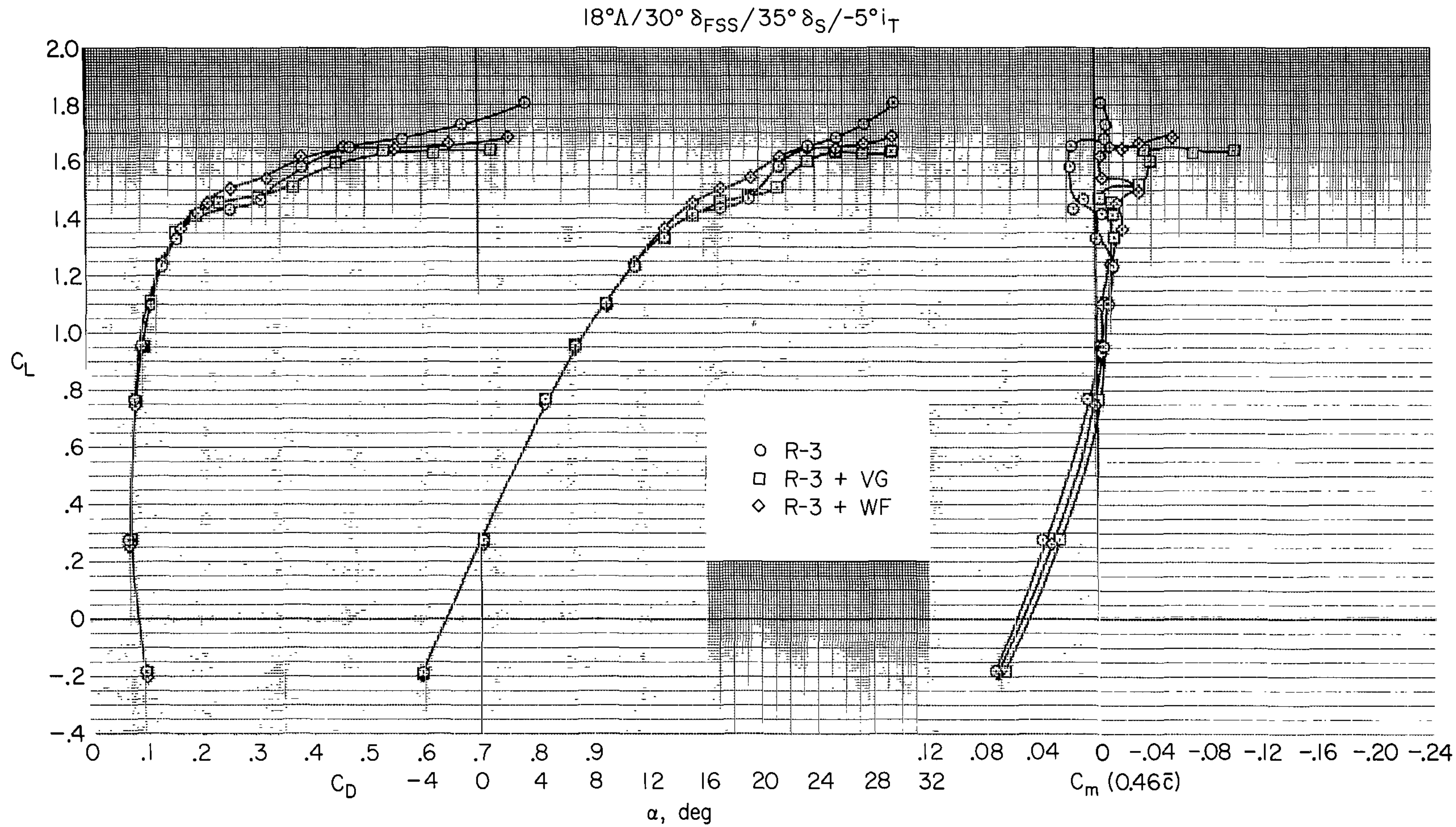

(a) Vortex generators and wing fence separately.

Figure 5.- Effects of flow control devices on the model with a constant (large) radius strake leading edge; 18° wing sweep.

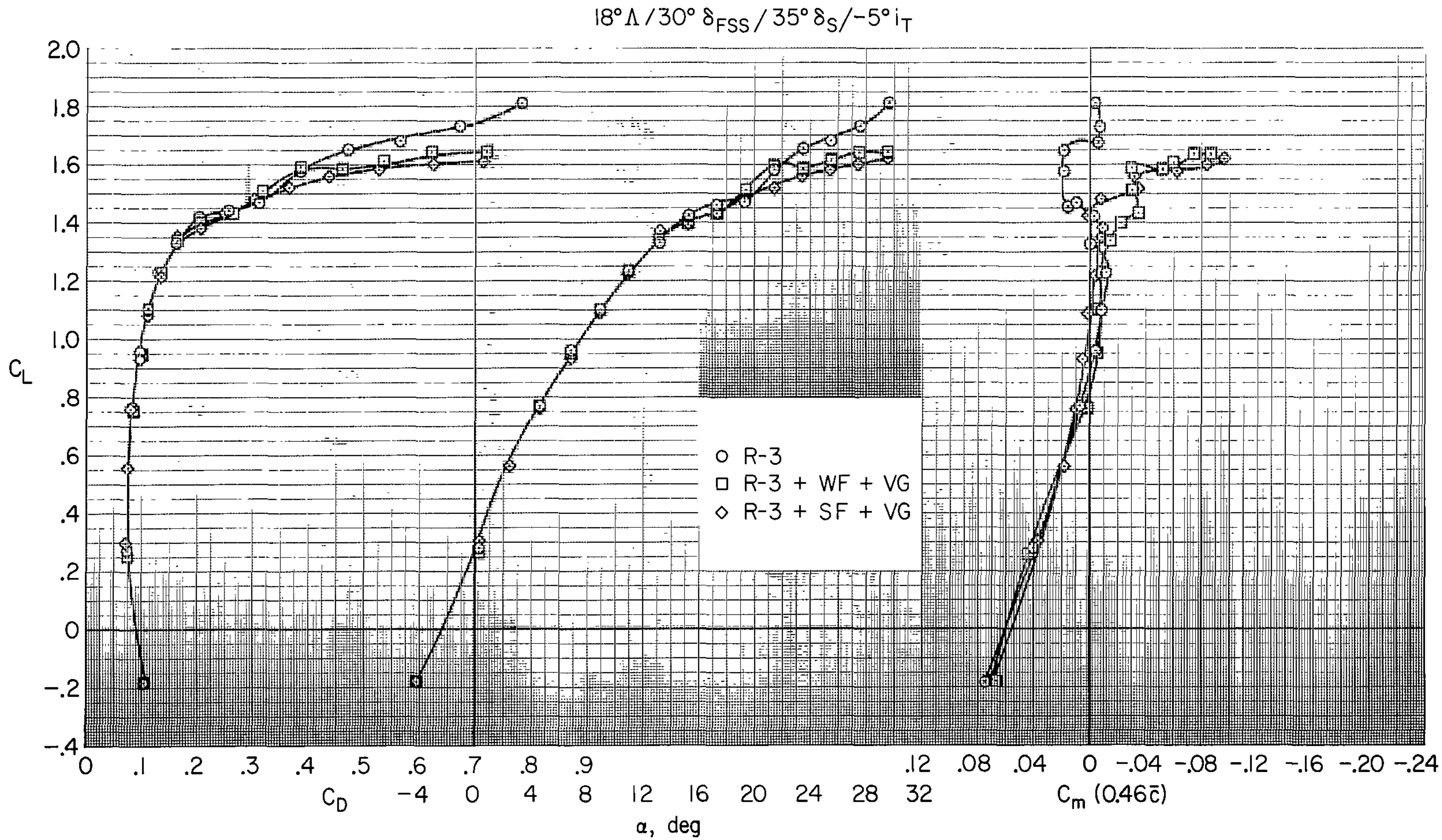

(b) Vortex generators and fences in combination.

Figure 5.- Continued.

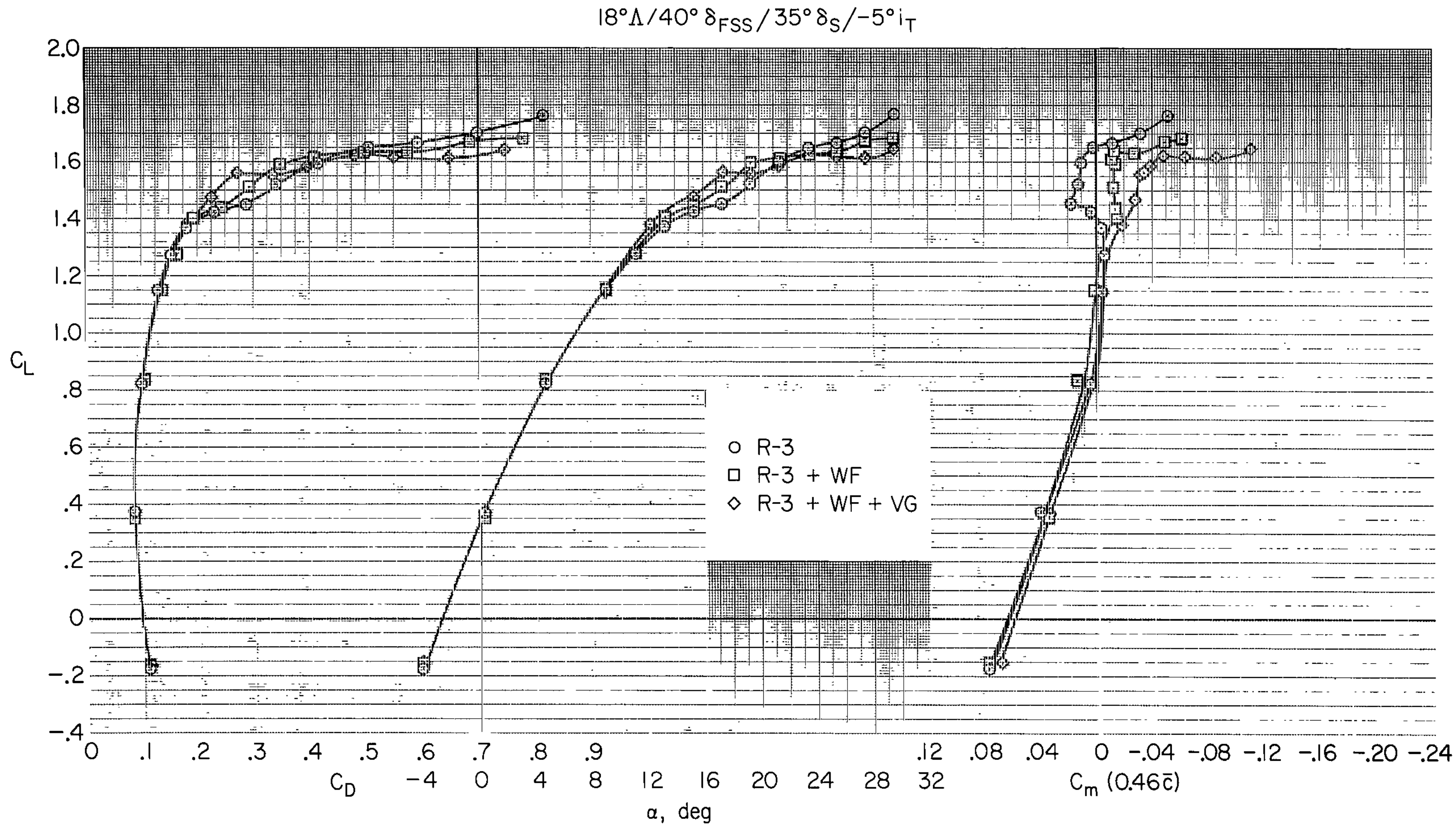

(c) Wing fence with vortex generators.

Figure 5.- Concluded.

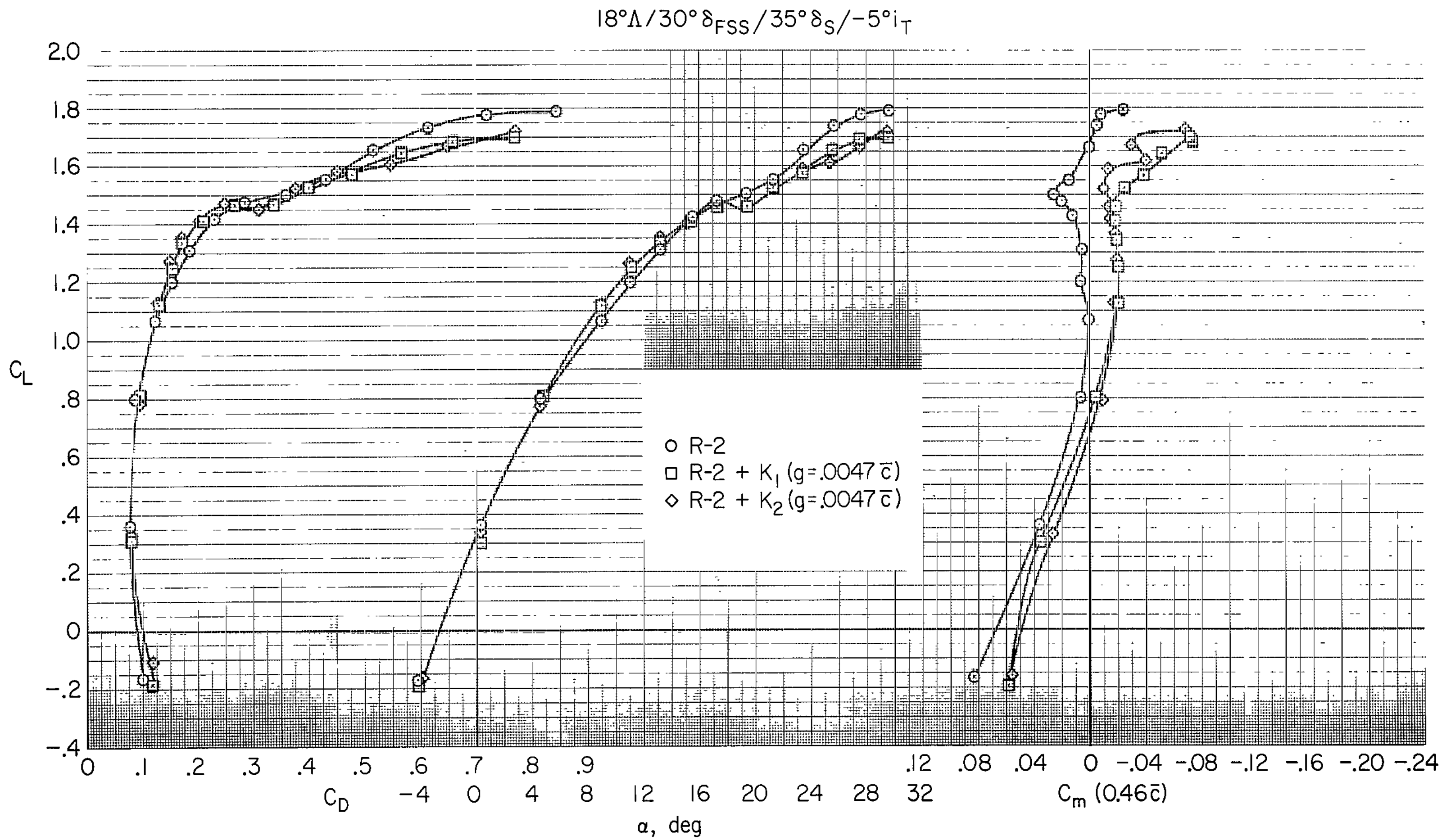

(a) K_1 and K_2.

Figure 6.- Effects of leading-edge flaps on the tapered radius strake leading edge; 18° wing sweep.

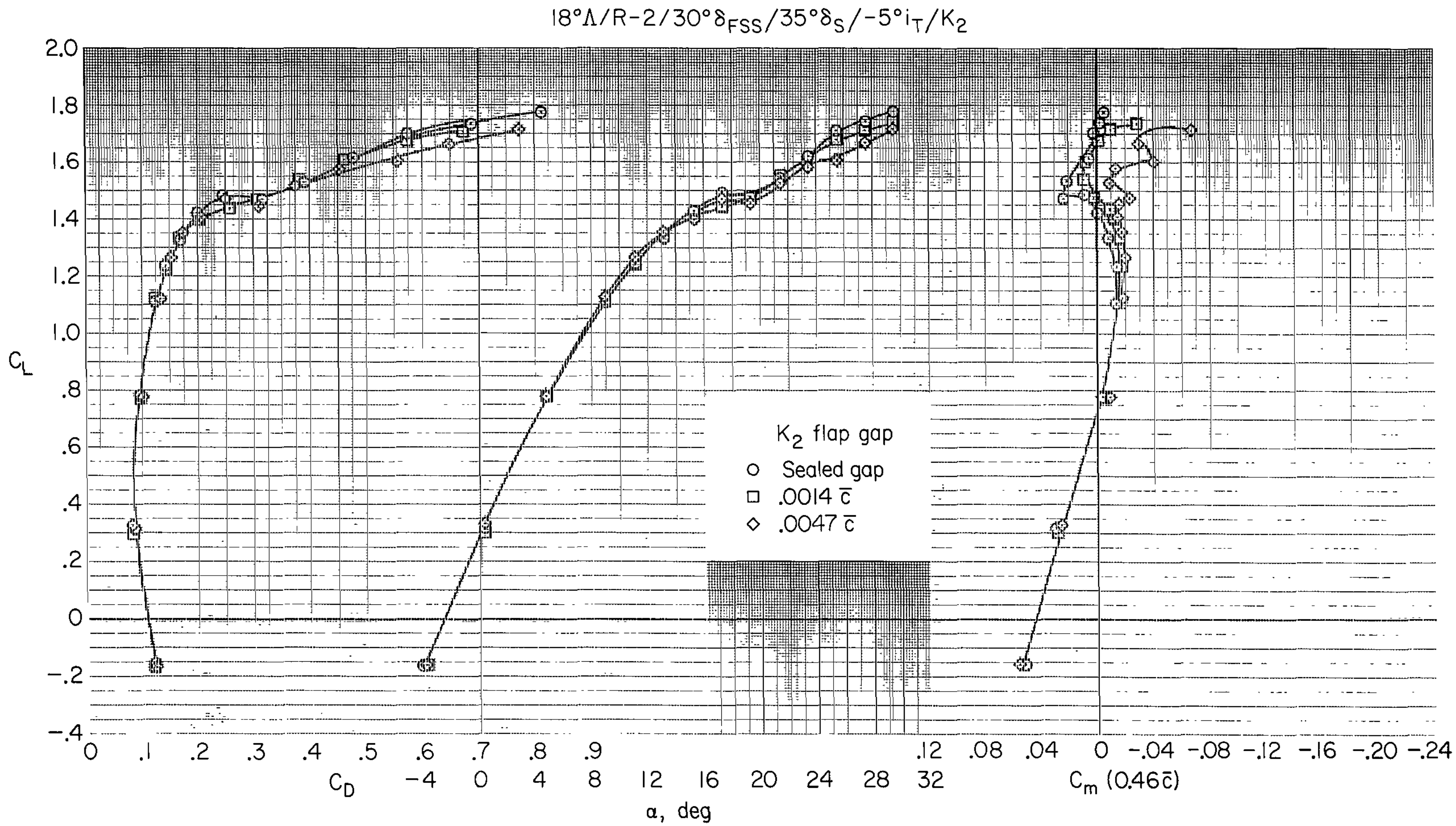

(b) K_2 gap.

Figure 6.- Continued.

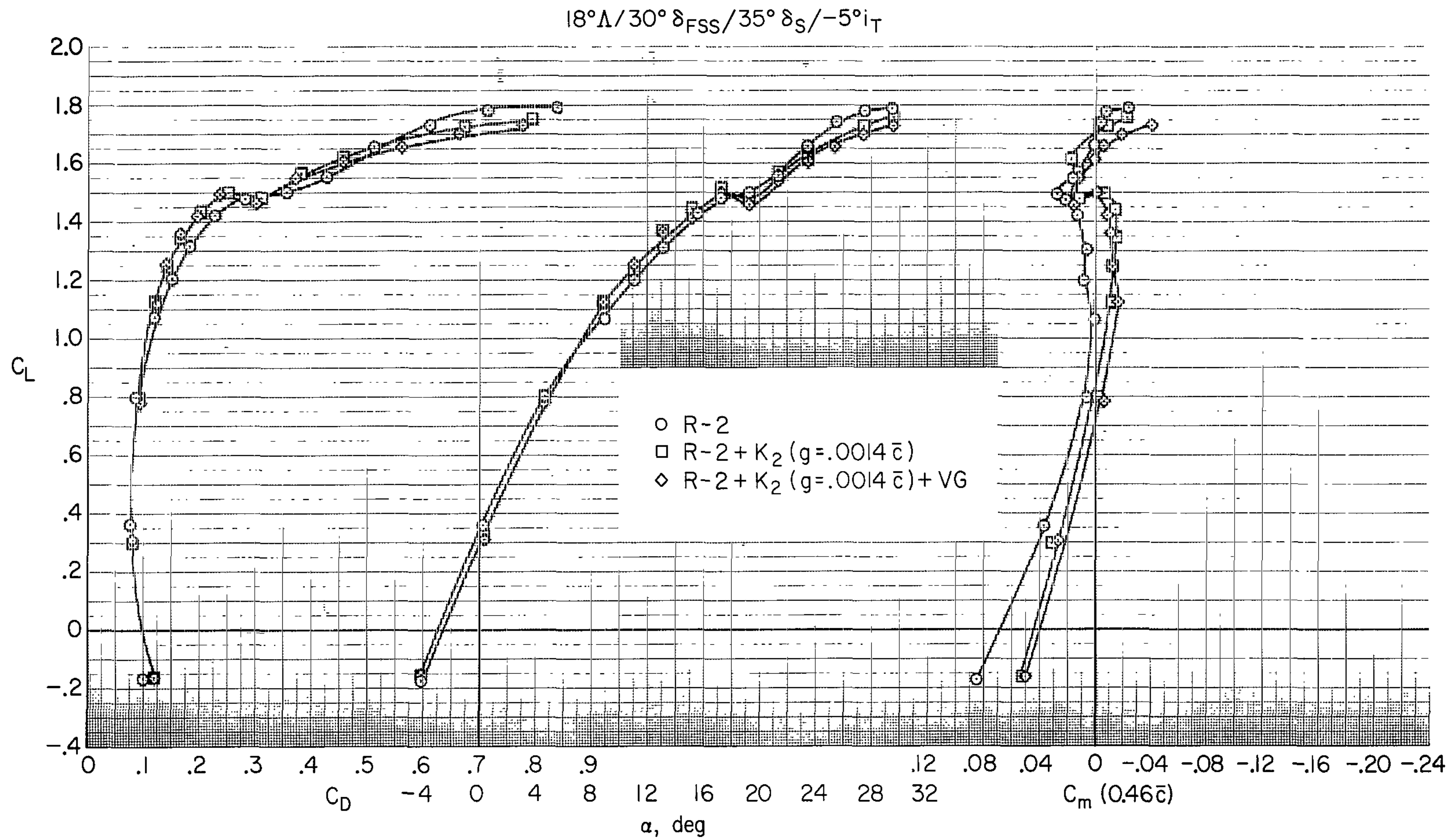

(c) K_2 with vortex generators.

Figure 6.- Continued.

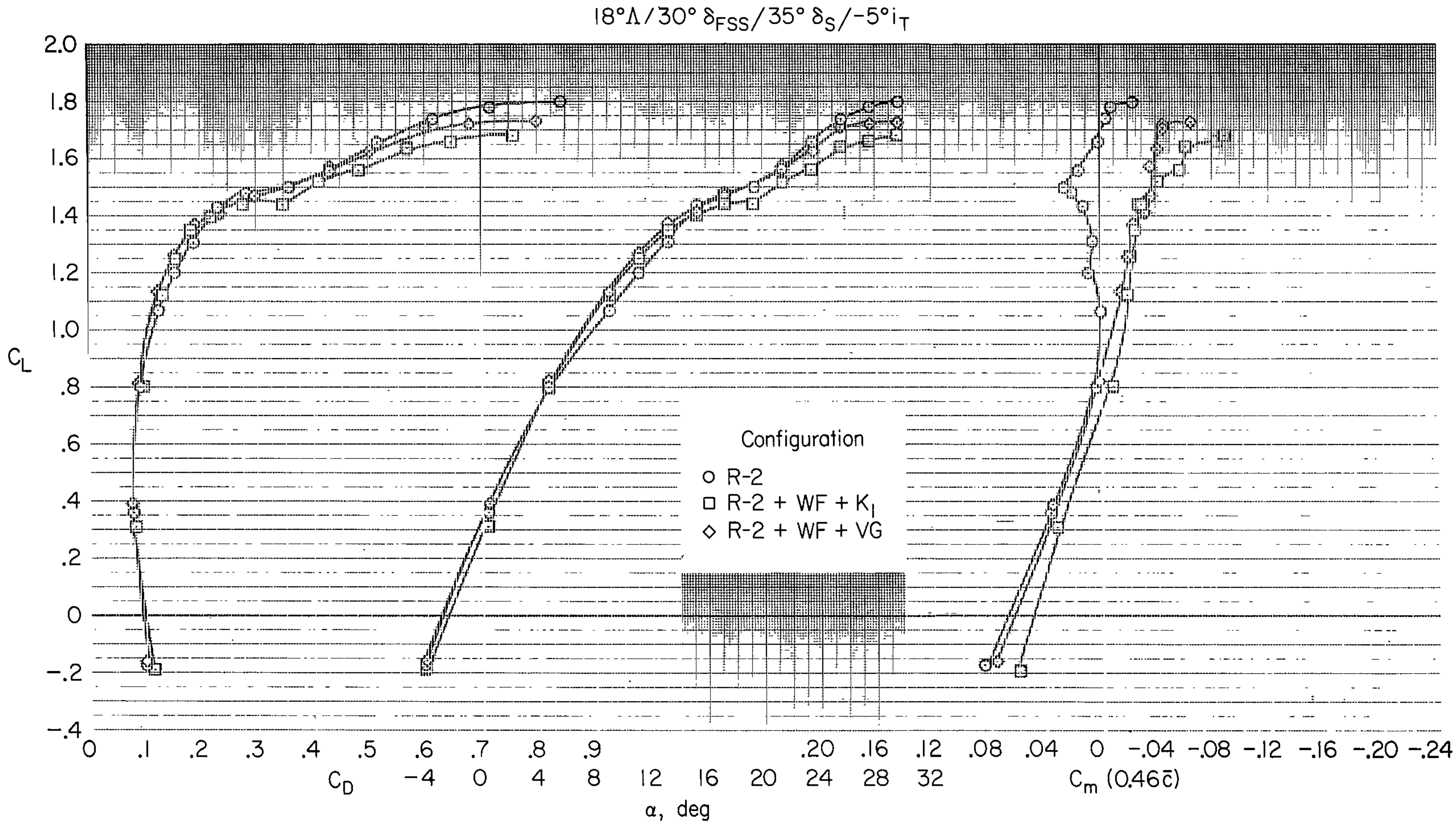

(d) K_1 with wing fence.

Figure 6.- Concluded.

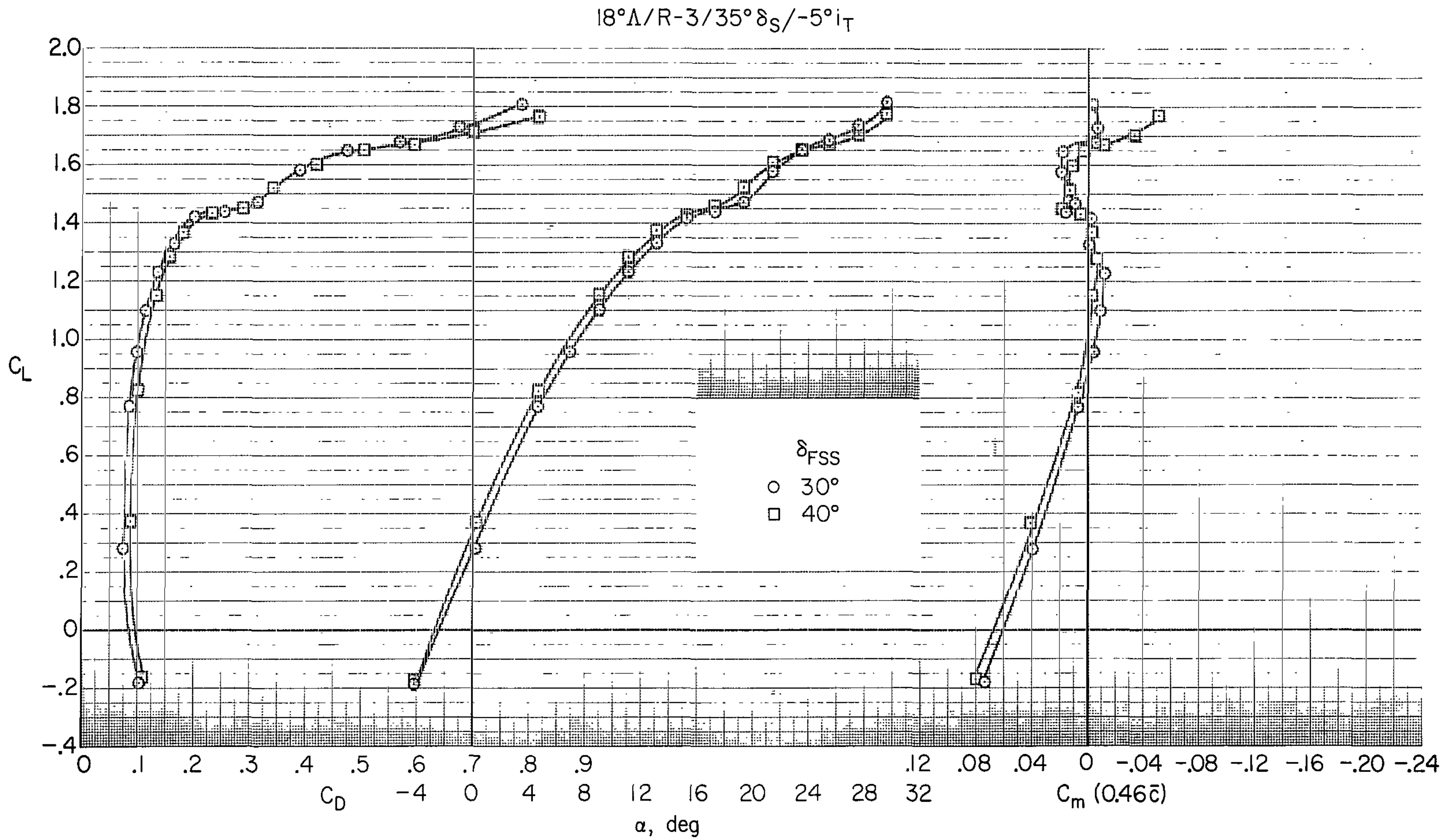

(a) With no strake flow control devices.

Figure 7.- Longitudinal characteristics of single-slotted flap deflection, with constant strake leading-edge radius; 18° wing sweep.

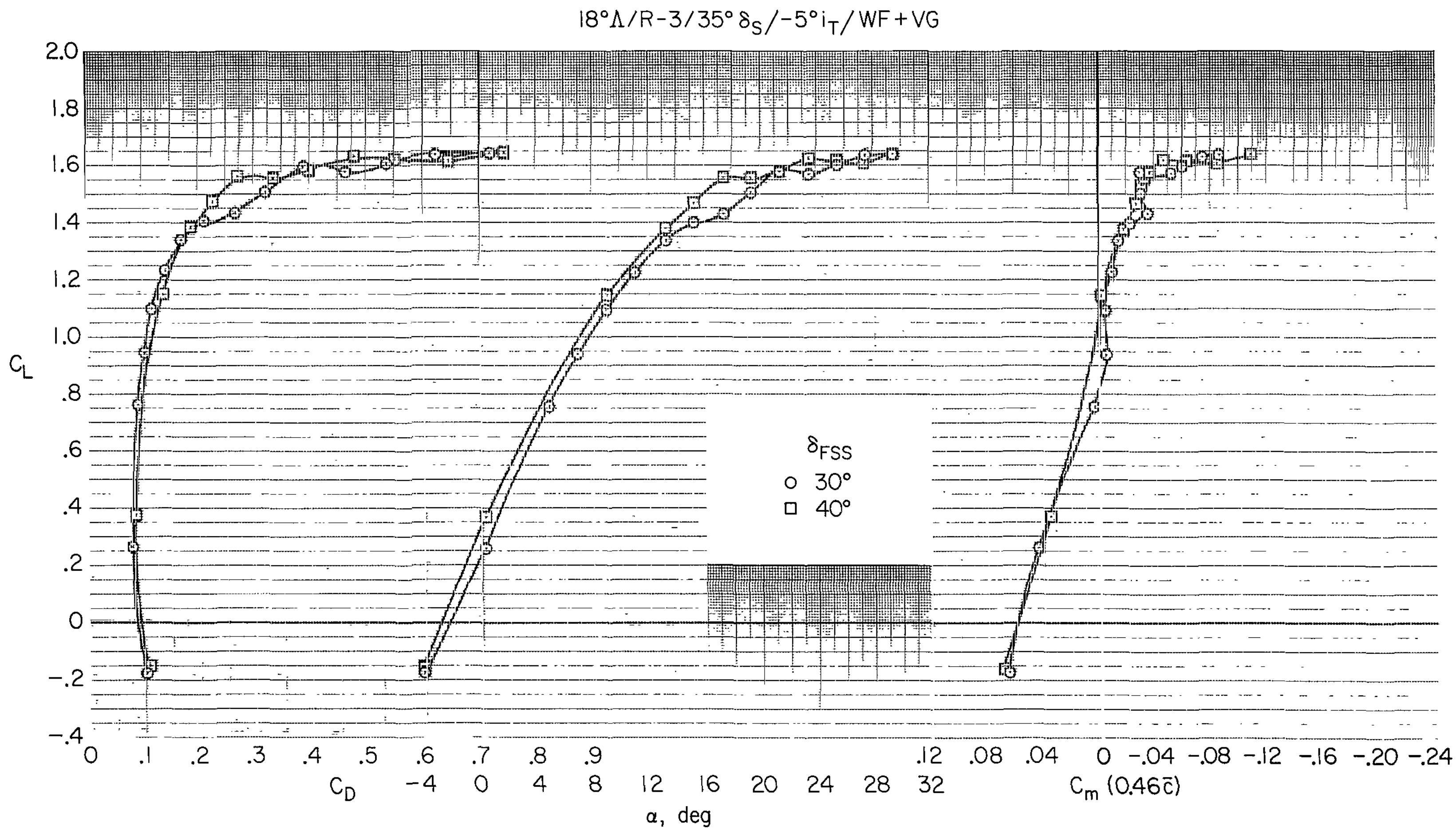

(b) With wing fence and vortex generators.

Figure 7.- Concluded.

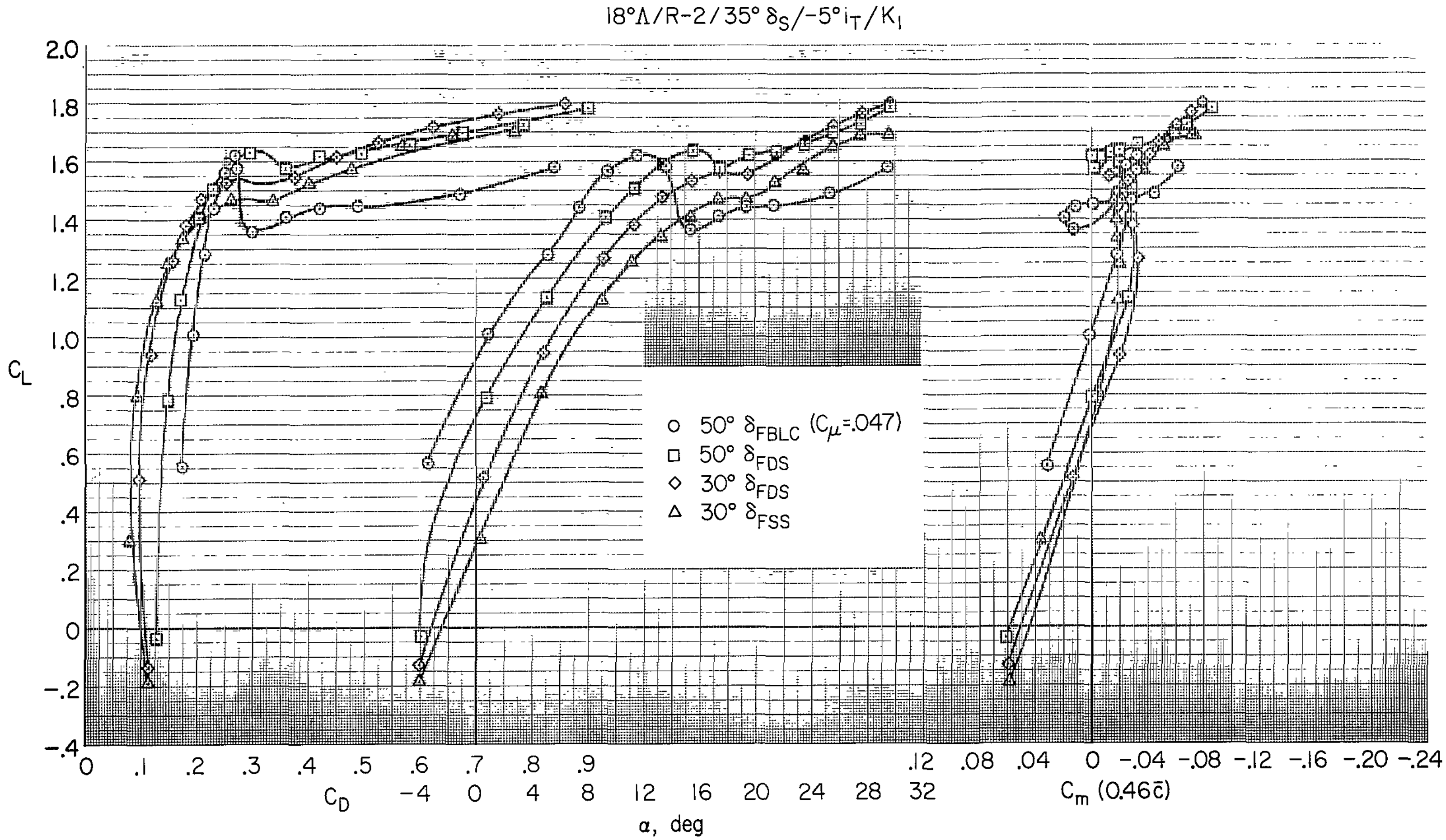

(a) With K_1.

Figure 8.- Characteristics of single-slotted, double-slotted, and BLC flaps, with tapered radius strake leading edge; 18° wing sweep.

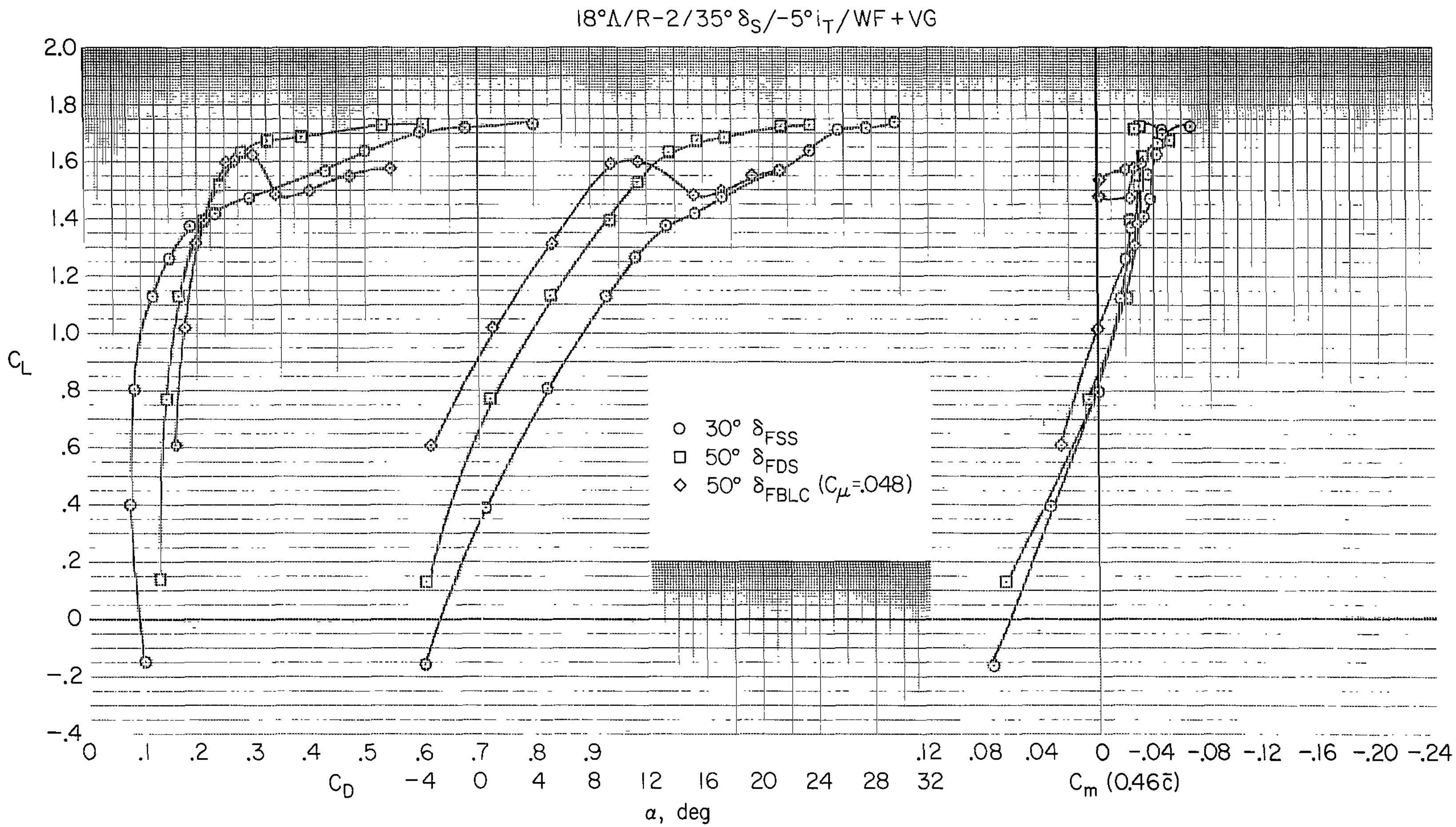

(b) With wing fence and vortex generators.

Figure 8.- Continued.

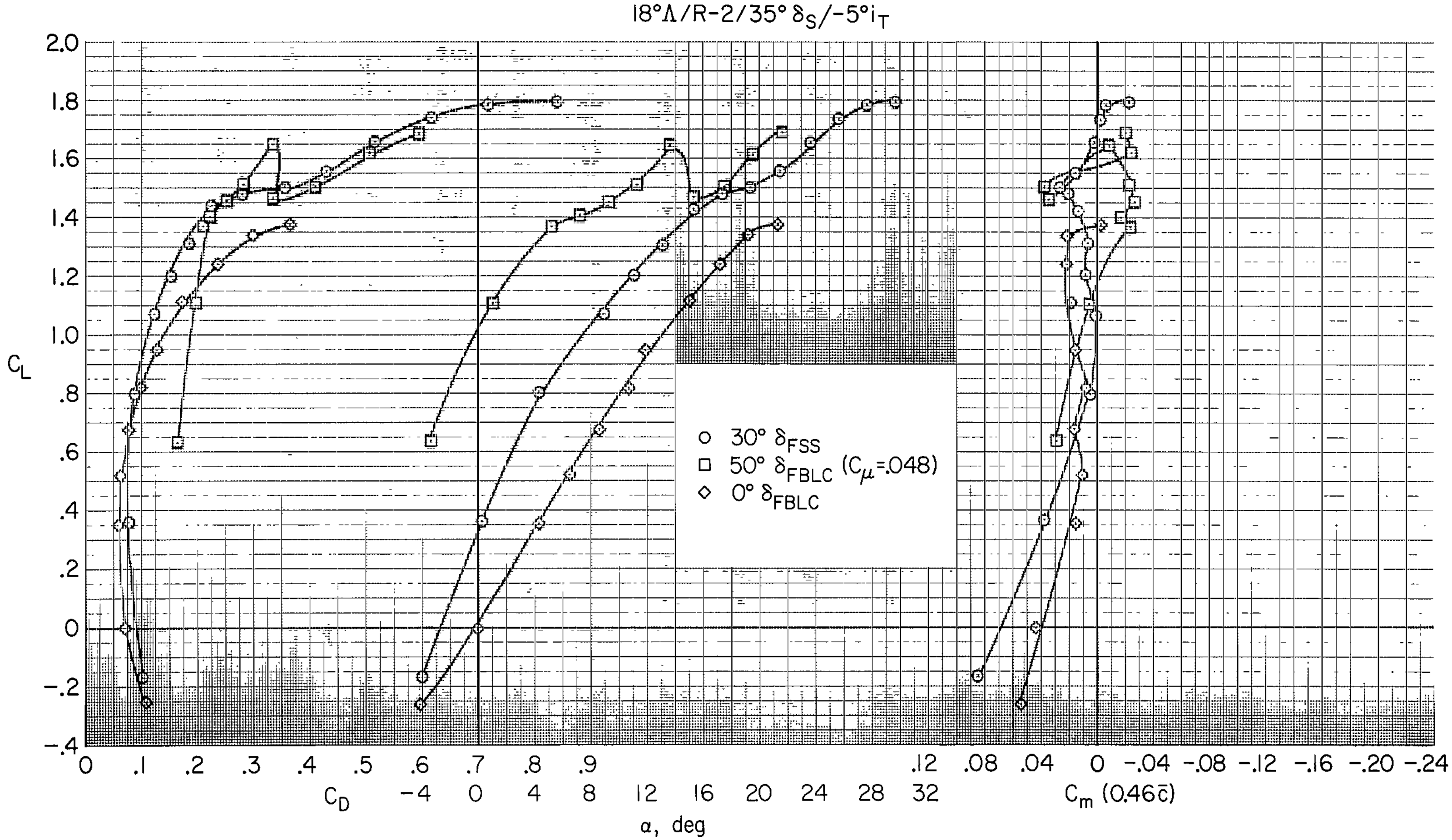

(c) With no strake flow control devices.

Figure 8.- Concluded.

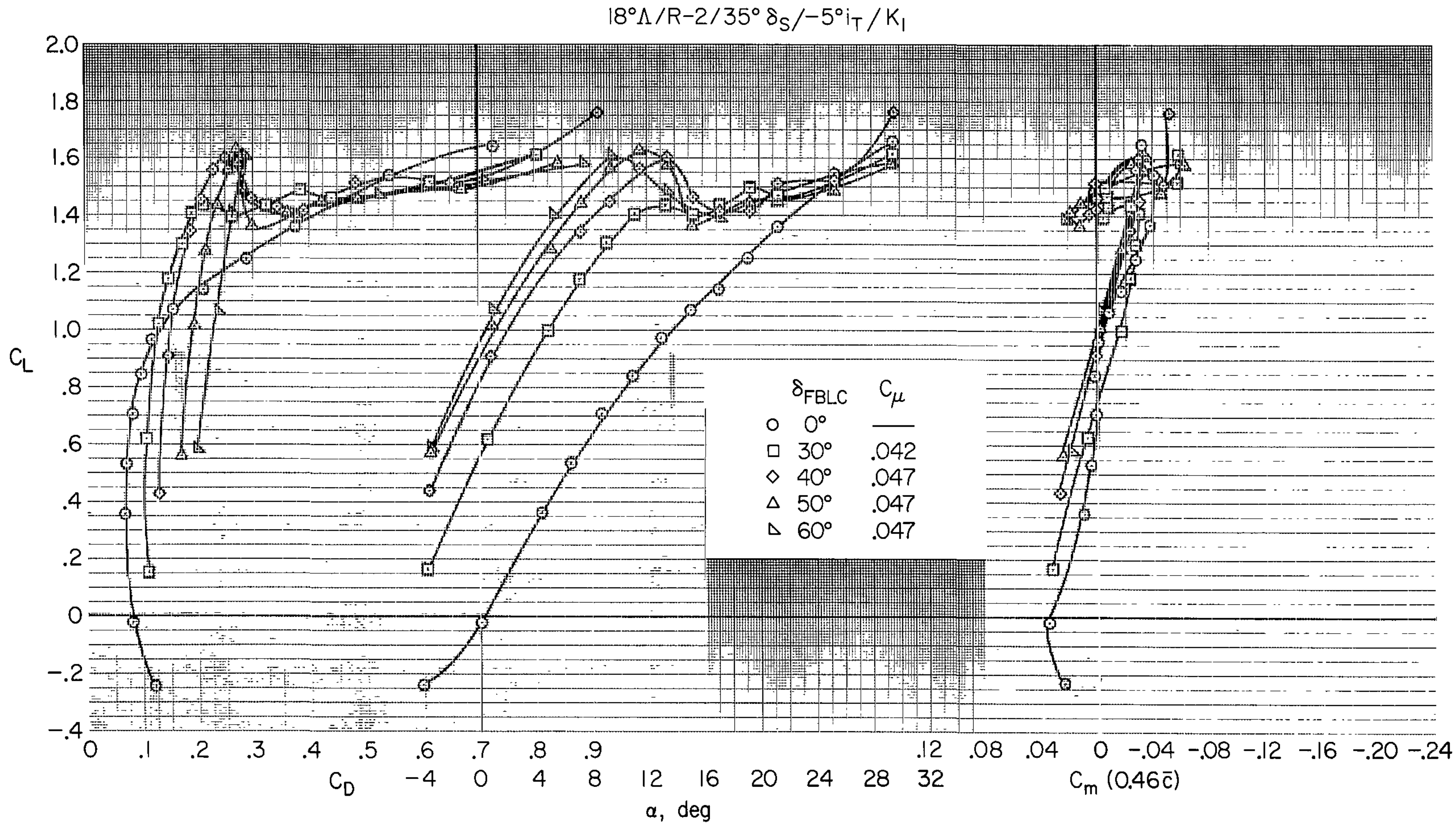

(a) Variable flap deflection.

Figure 9.- Effects of BLC flap deflection and momentum coefficient, constant-chord strake leading-edge flap, tapered radius strake leading edge; 18° wing sweep.

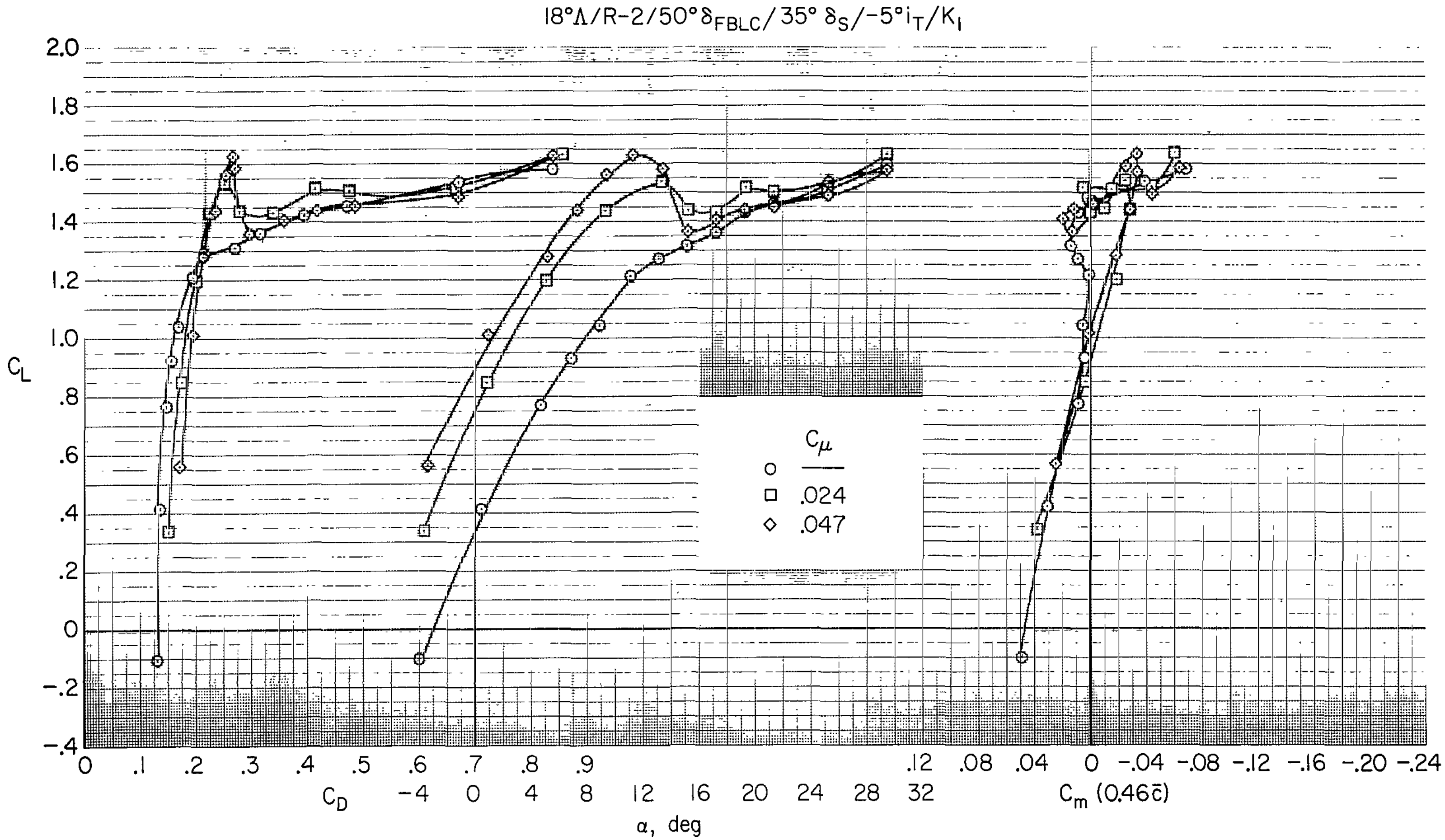

(b) Variable momentum coefficient.

Figure 9.- Concluded.

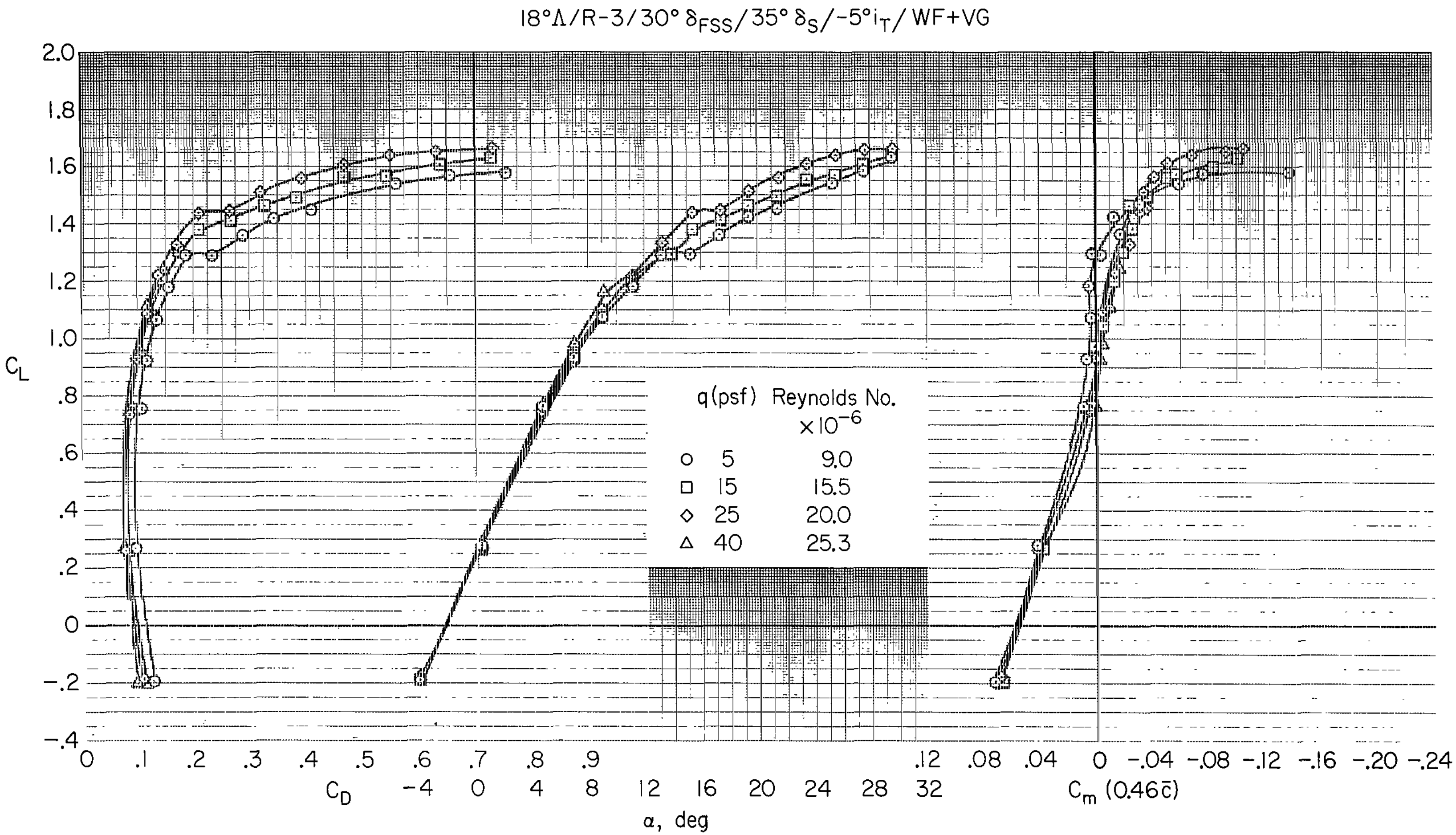

Figure 10.- Effects of Reynolds number on longitudinal characteristics; 18° wing sweep.

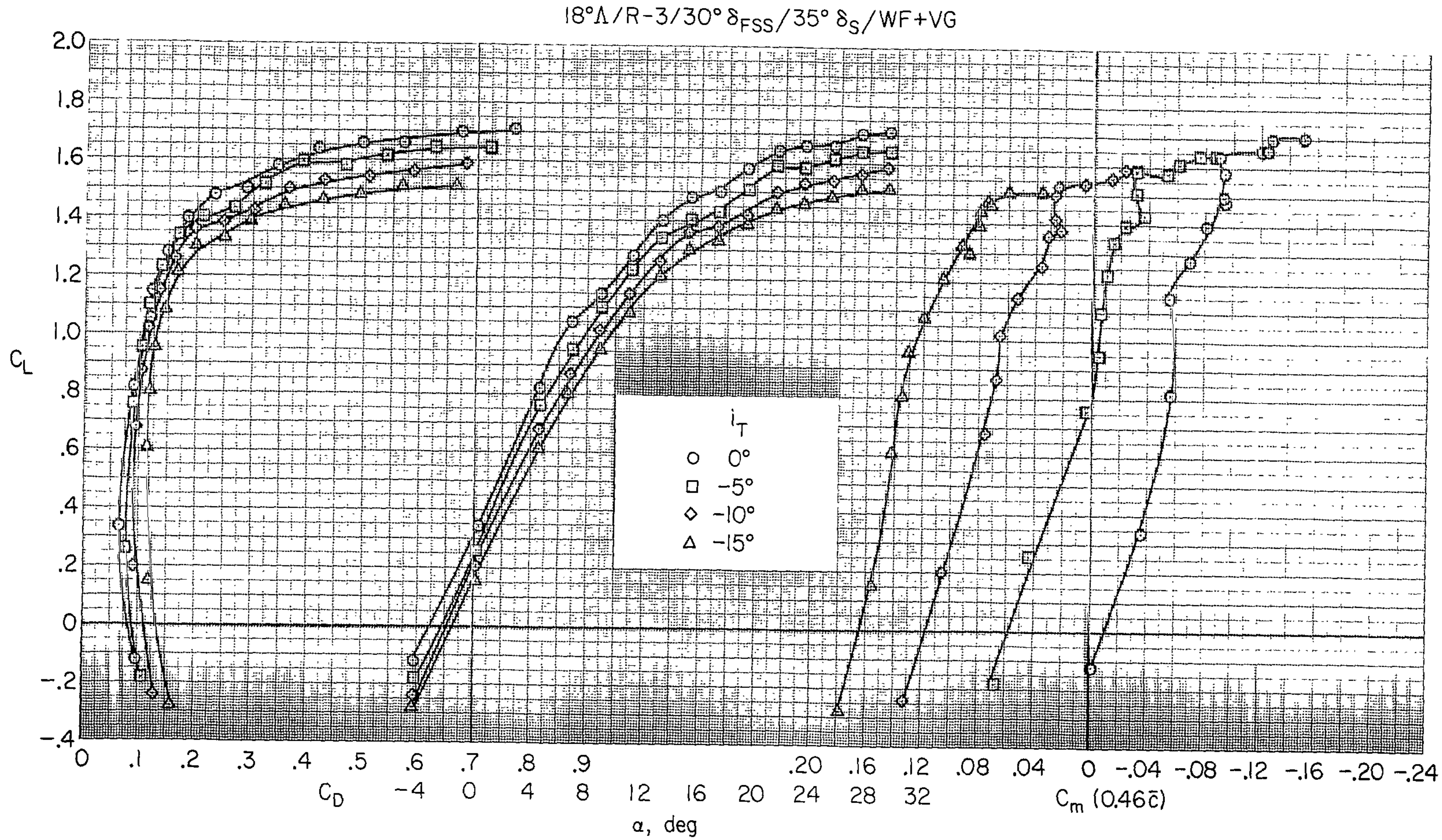

Figure 11.- Effects of horizontal-tail incidence; 18° wing sweep.

44

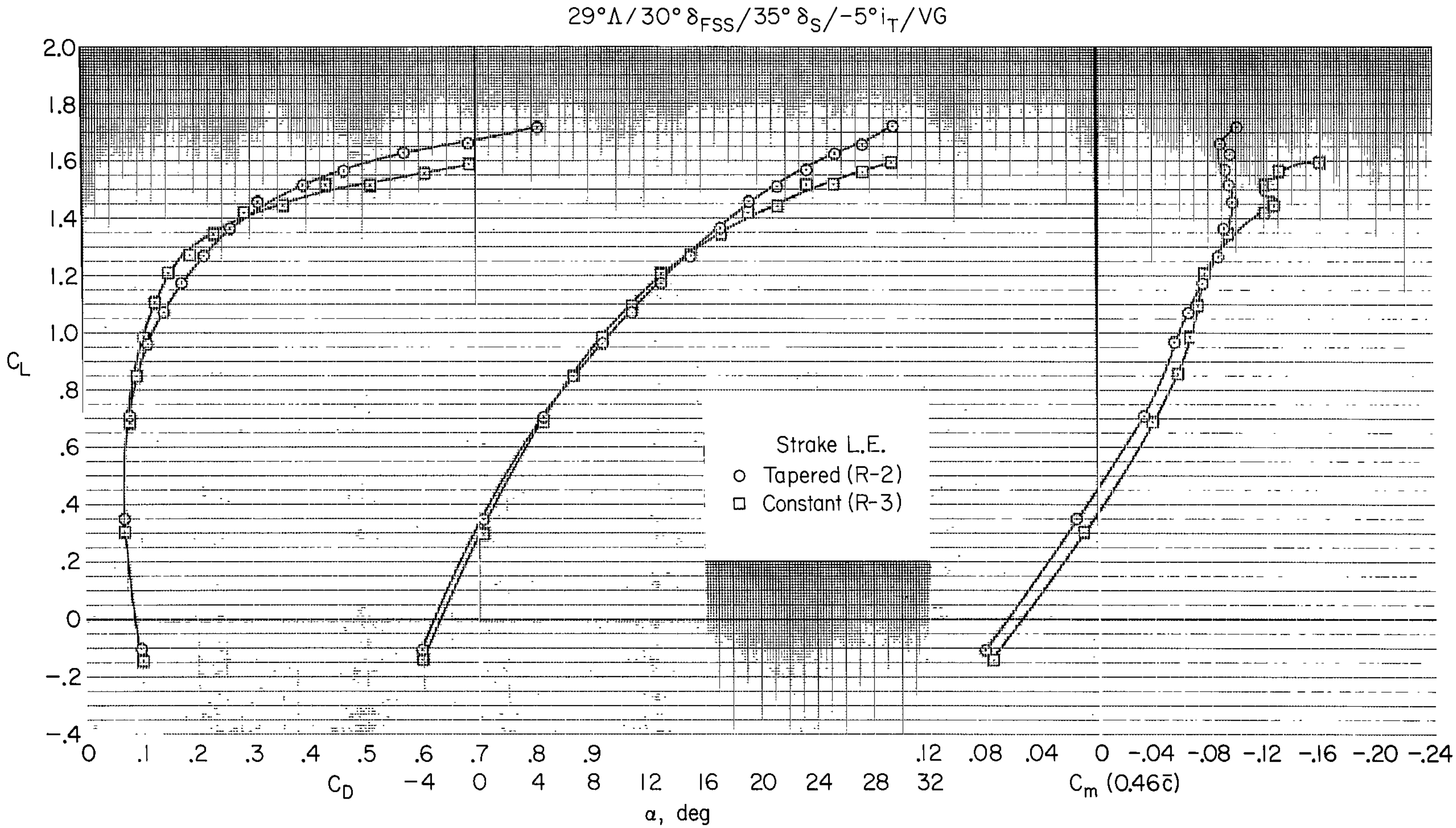

Figure 12.- Effects of strake leading-edge radius with vortex generators; 29° wing sweep.

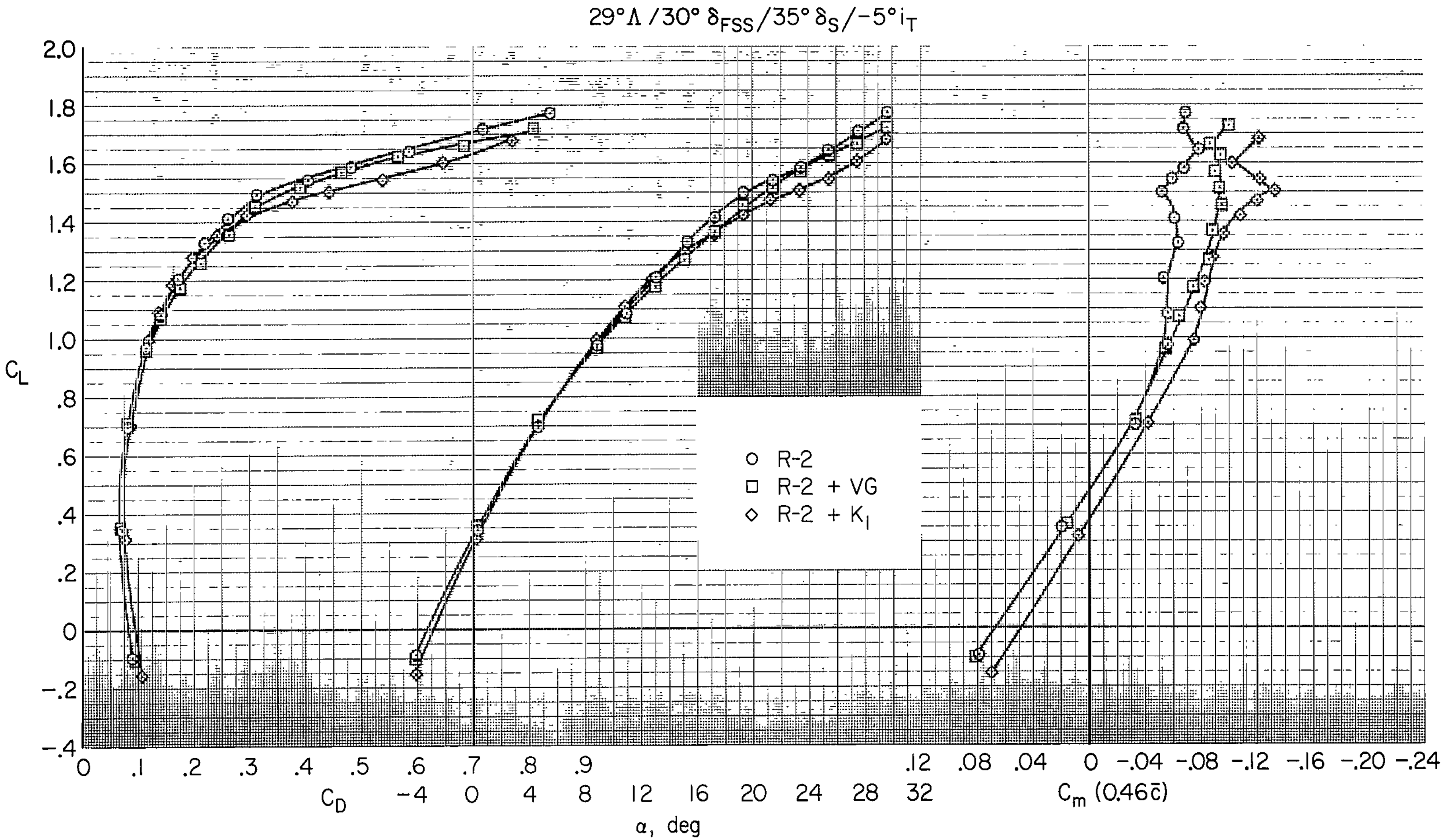

Figure 13.- Effects of vortex generators and strake leading-edge flap, with tapered radius strake leading edge; 29° wing sweep.

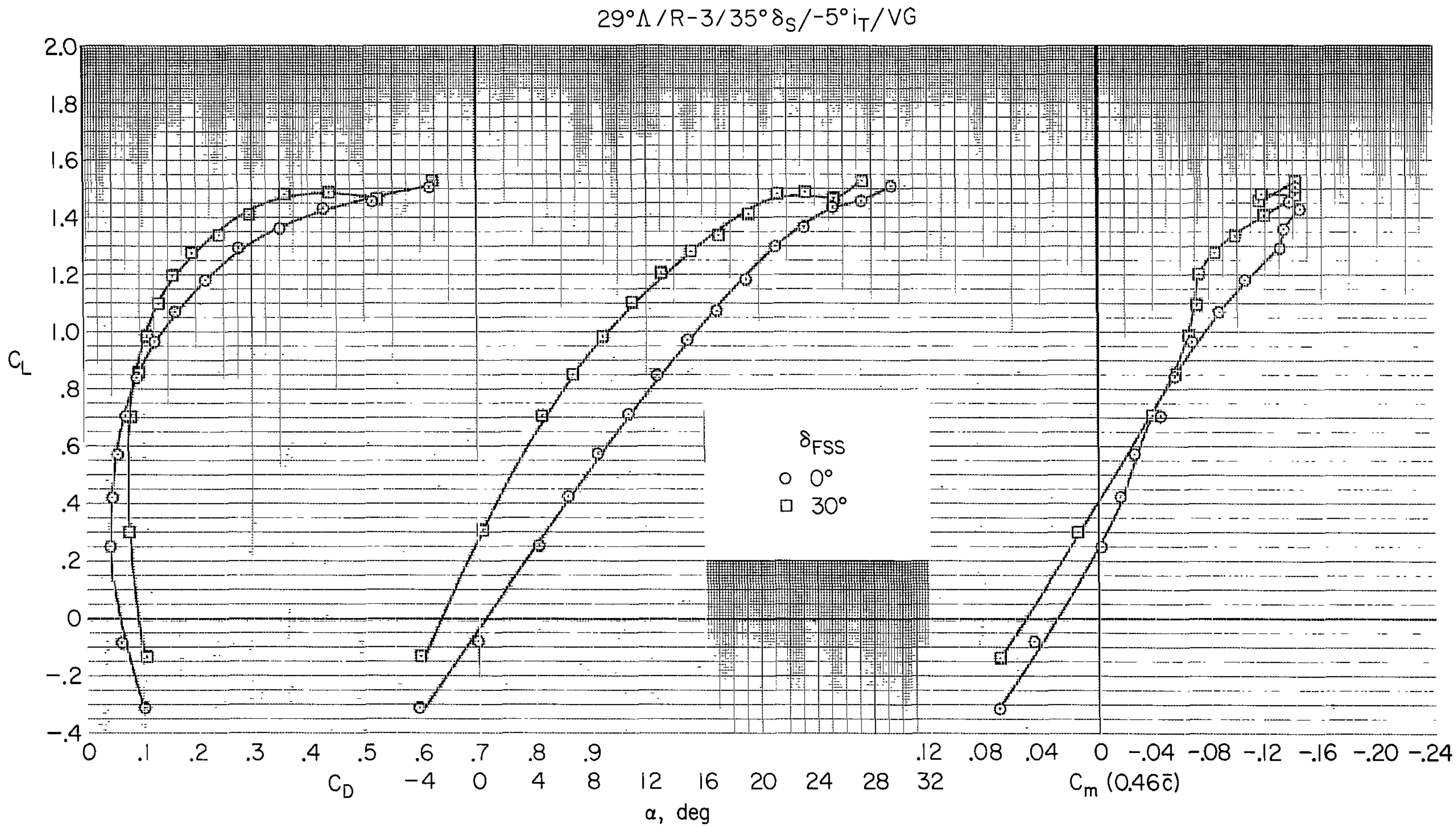

Figure 14.- Effect of single-slotted flap deflection with constant-radius strake leading edge and vortex generators; 29° wing sweep.

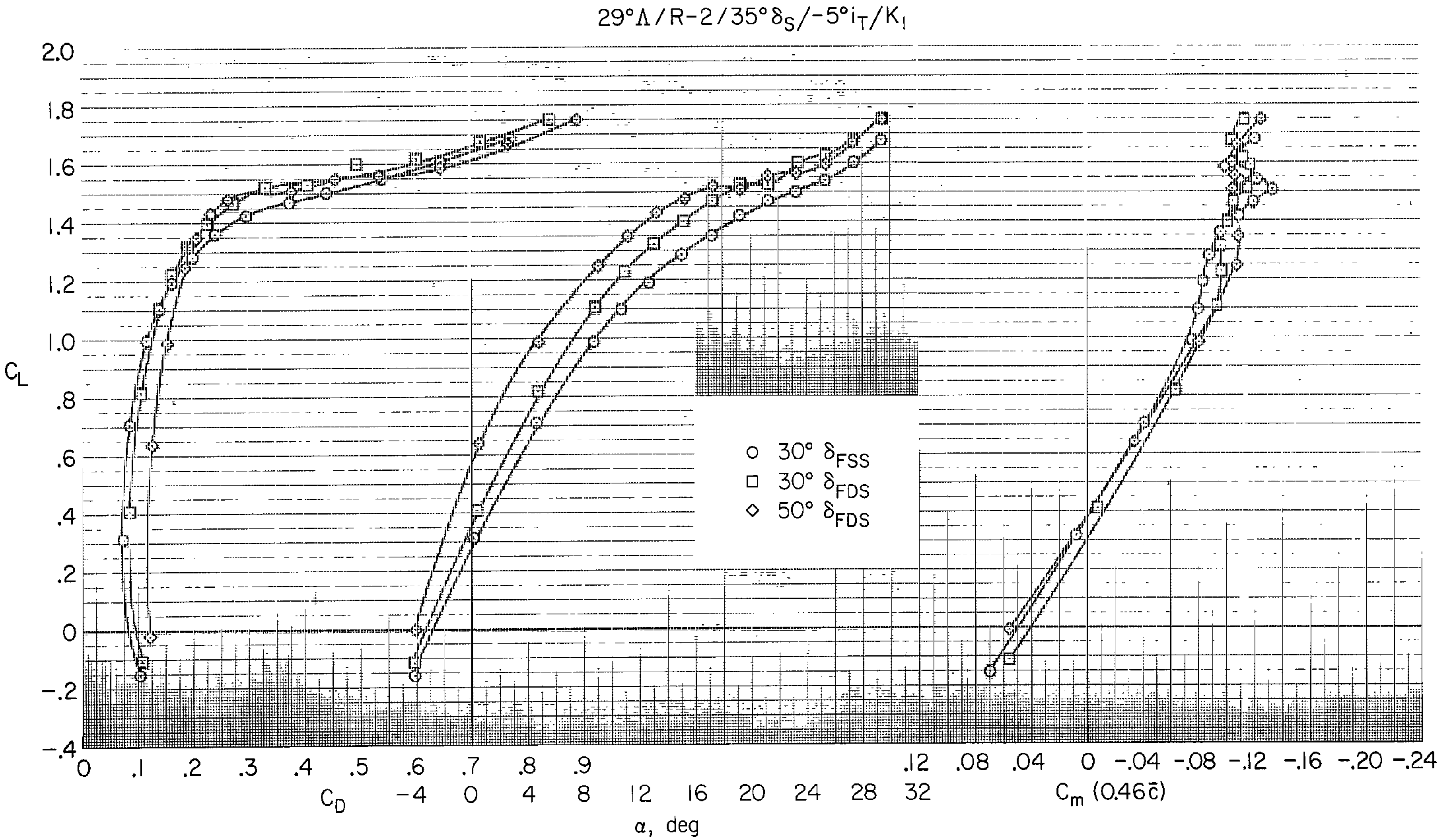

Figure 15.- Comparison of the aerodynamic characteristics of single- and double-slotted flap, with tapered radius strake leading edge, strake leading-edge flap; 29° wing sweep.

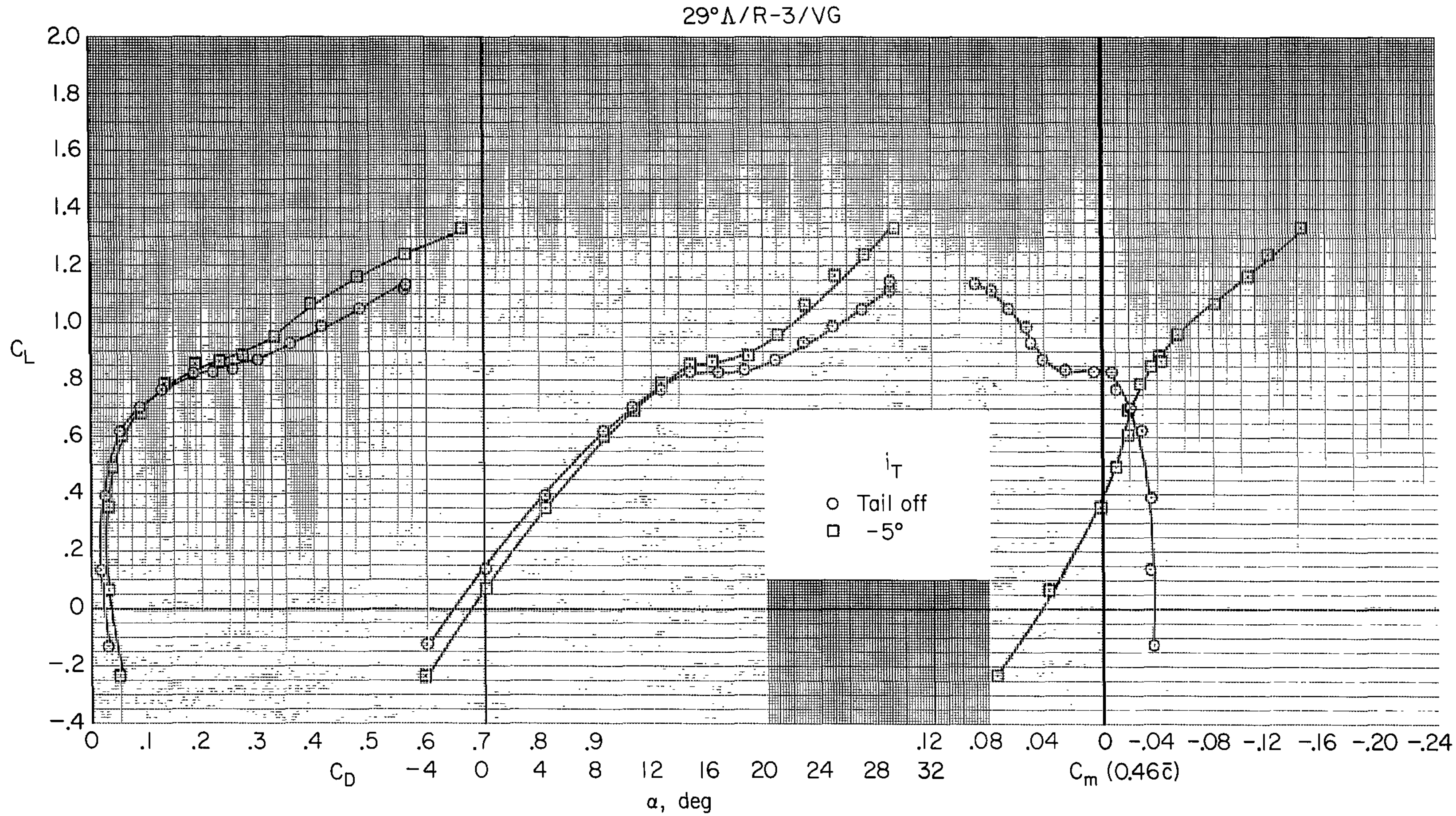

(a) Wing slats retracted and **flaps up.**

Figure 16.- Effects of horizontal-tail incidence on longitudinal characteristics; 29° wing sweep.

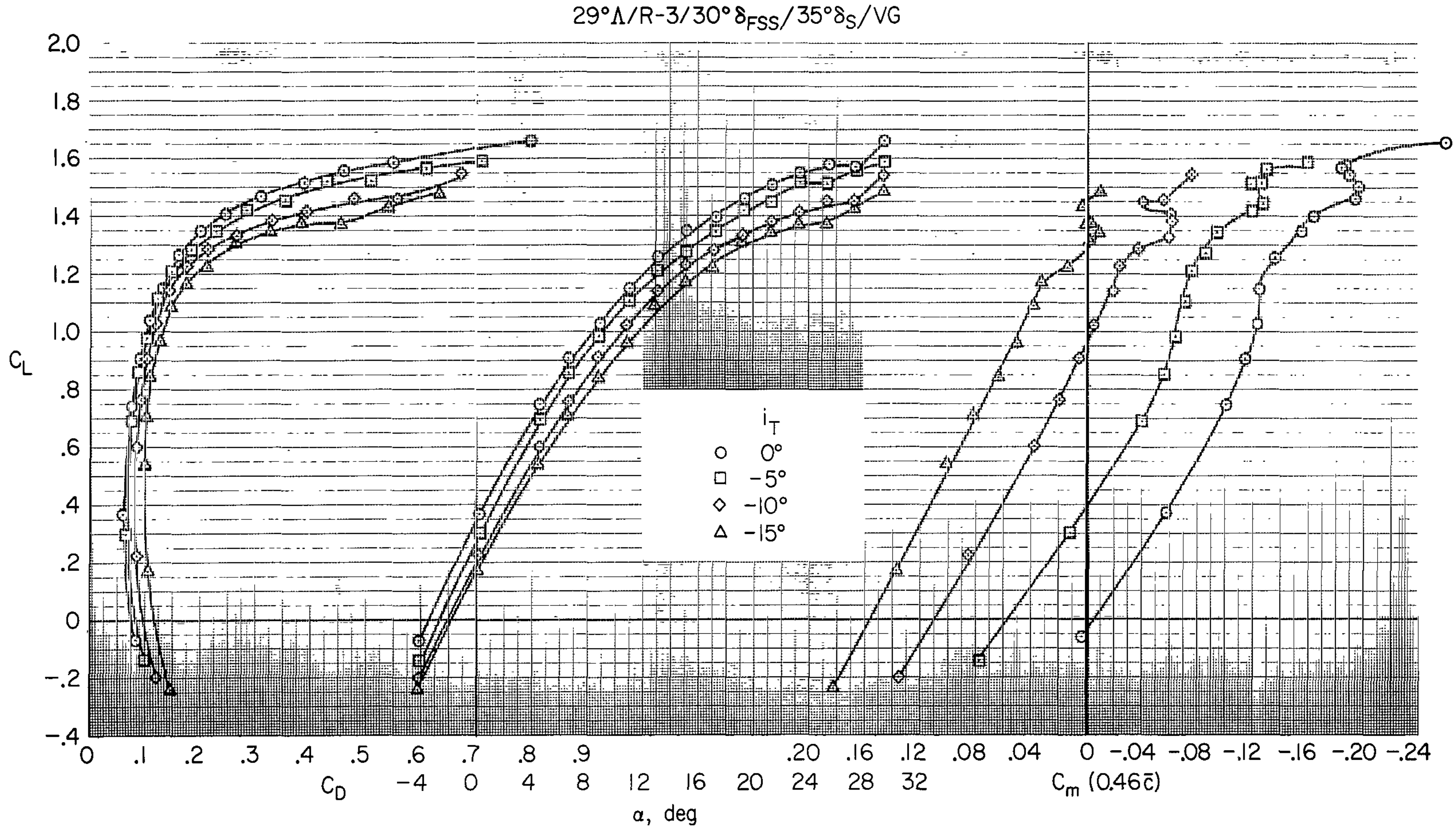

(b) 35° wing slats; 30° single-slotted flaps.

Figure 16.- Concluded.

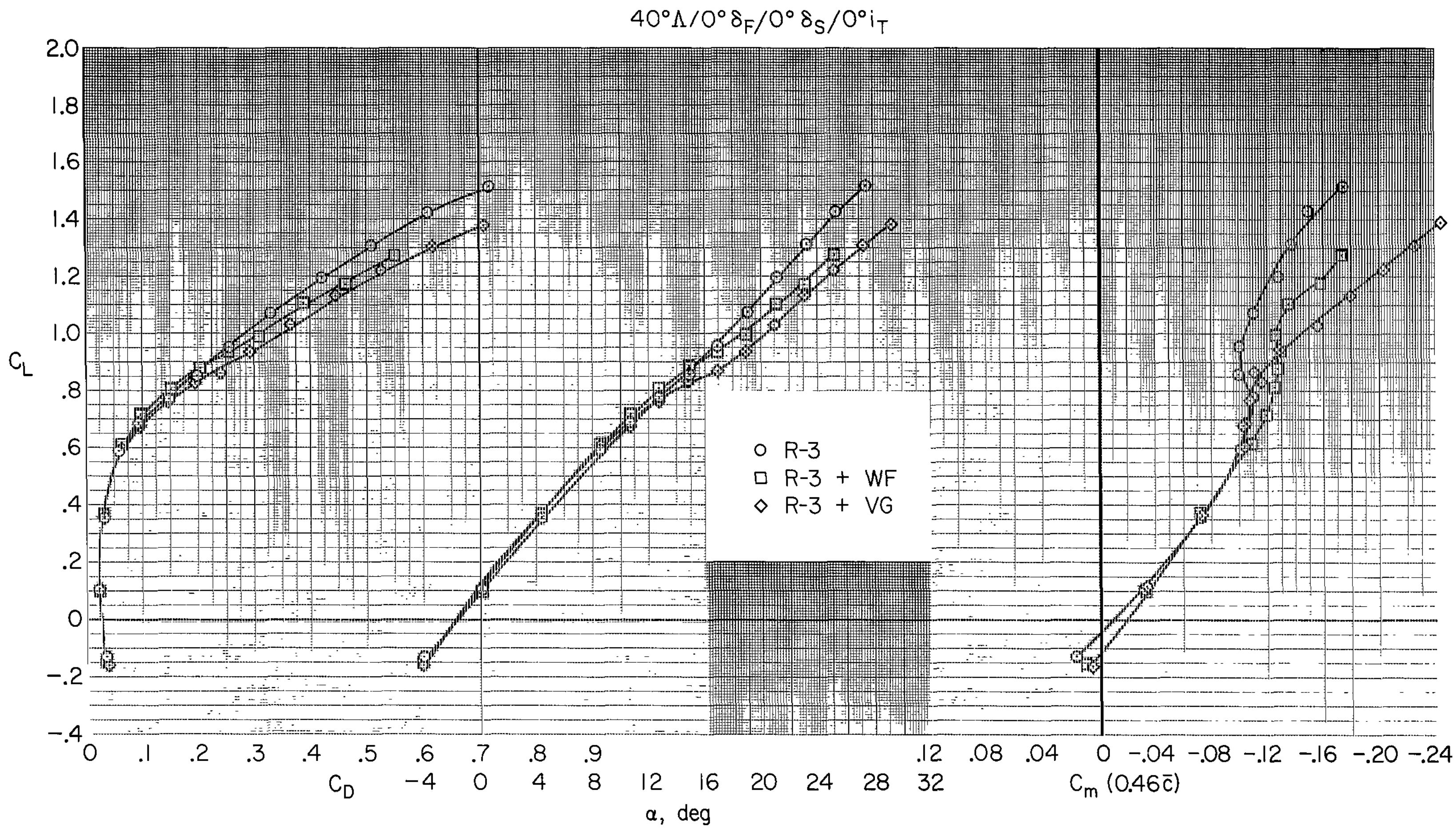

Figure 17.- Effects of wing fence and vortex generators with constant-radius strake leading edge; clean wing, 40° wing sweep.

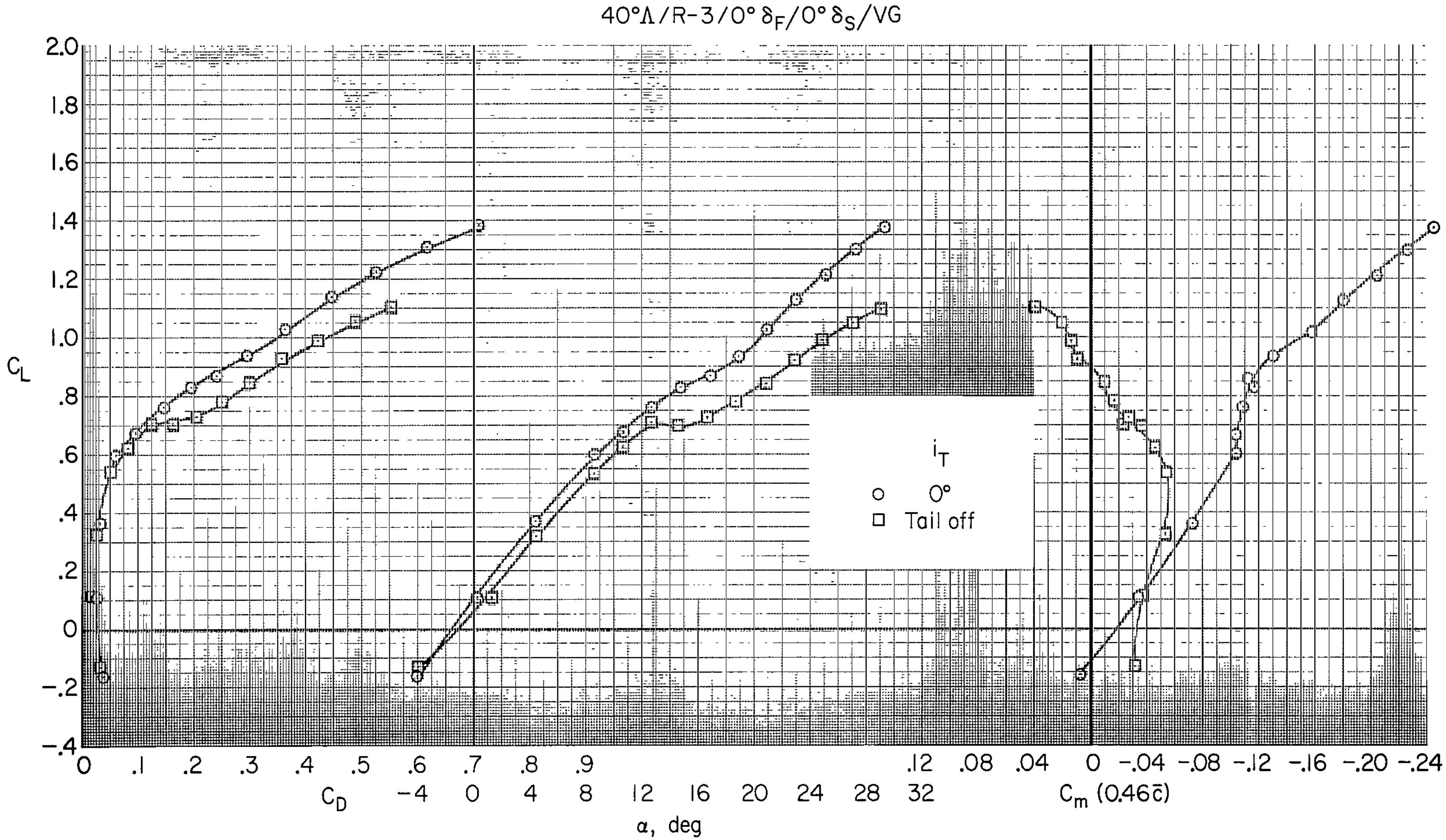

Figure 18.- Effect of horizontal tail on longitudinal characteristics; 40° wing sweep.

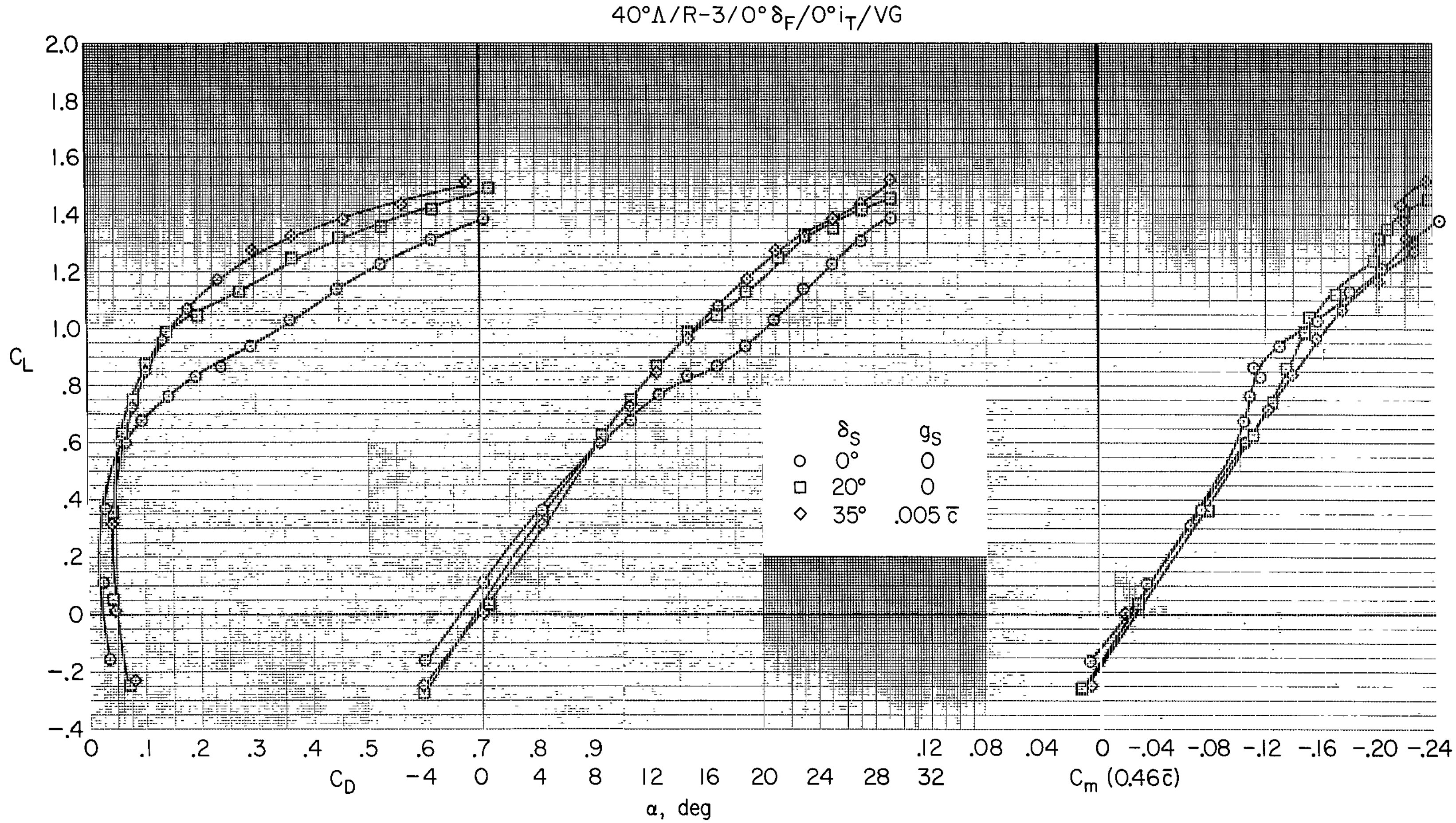

Figure 19.- Effect of leading-edge slat deflection with constant strake leading-edge radius, vortex generators, trailing-edge flaps up; 40° wing sweep.

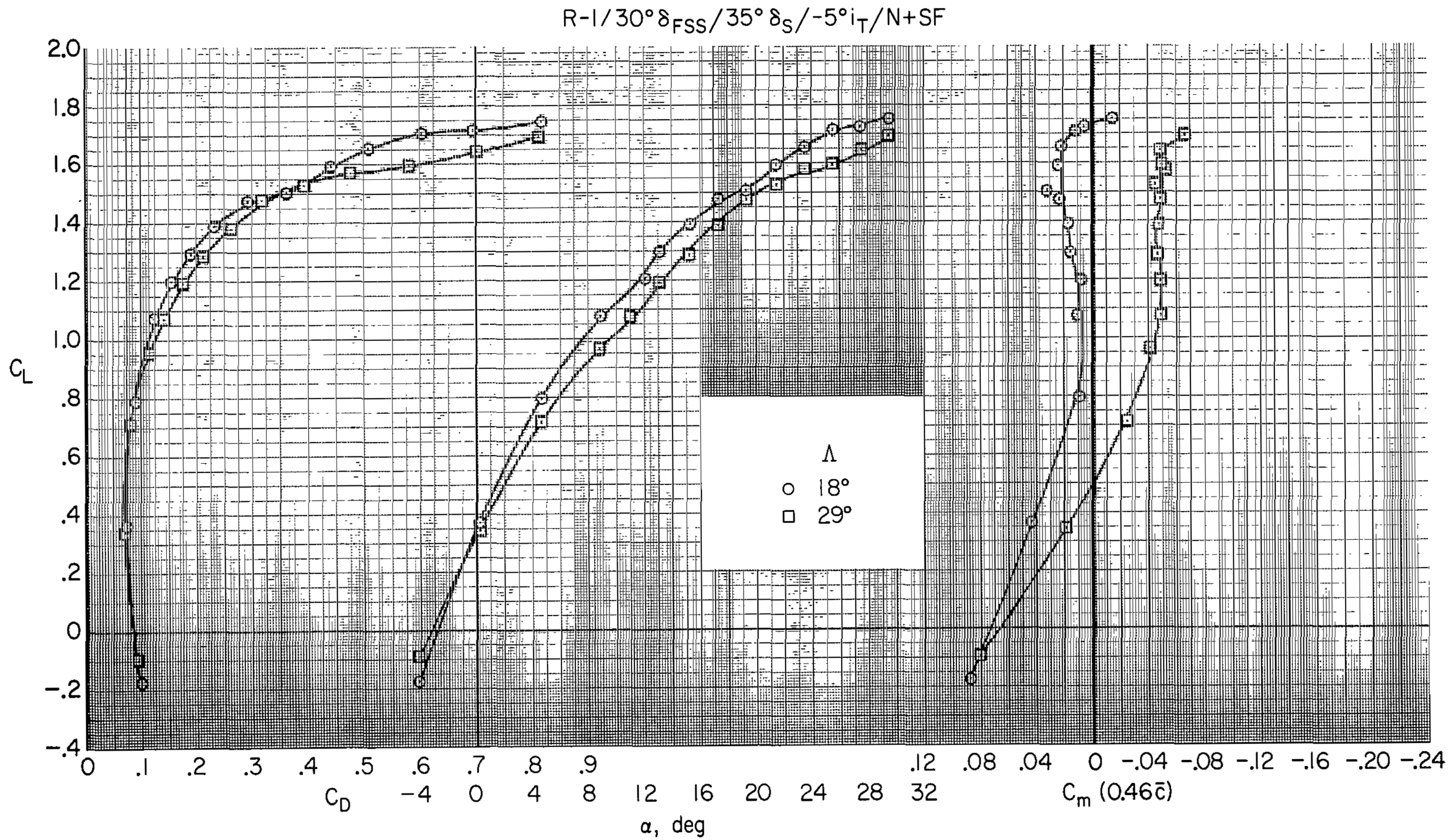

Figure 20.- Effect of wing sweepback angle, sharp strake leading edge, strake fence, and strake leading-edge notch.

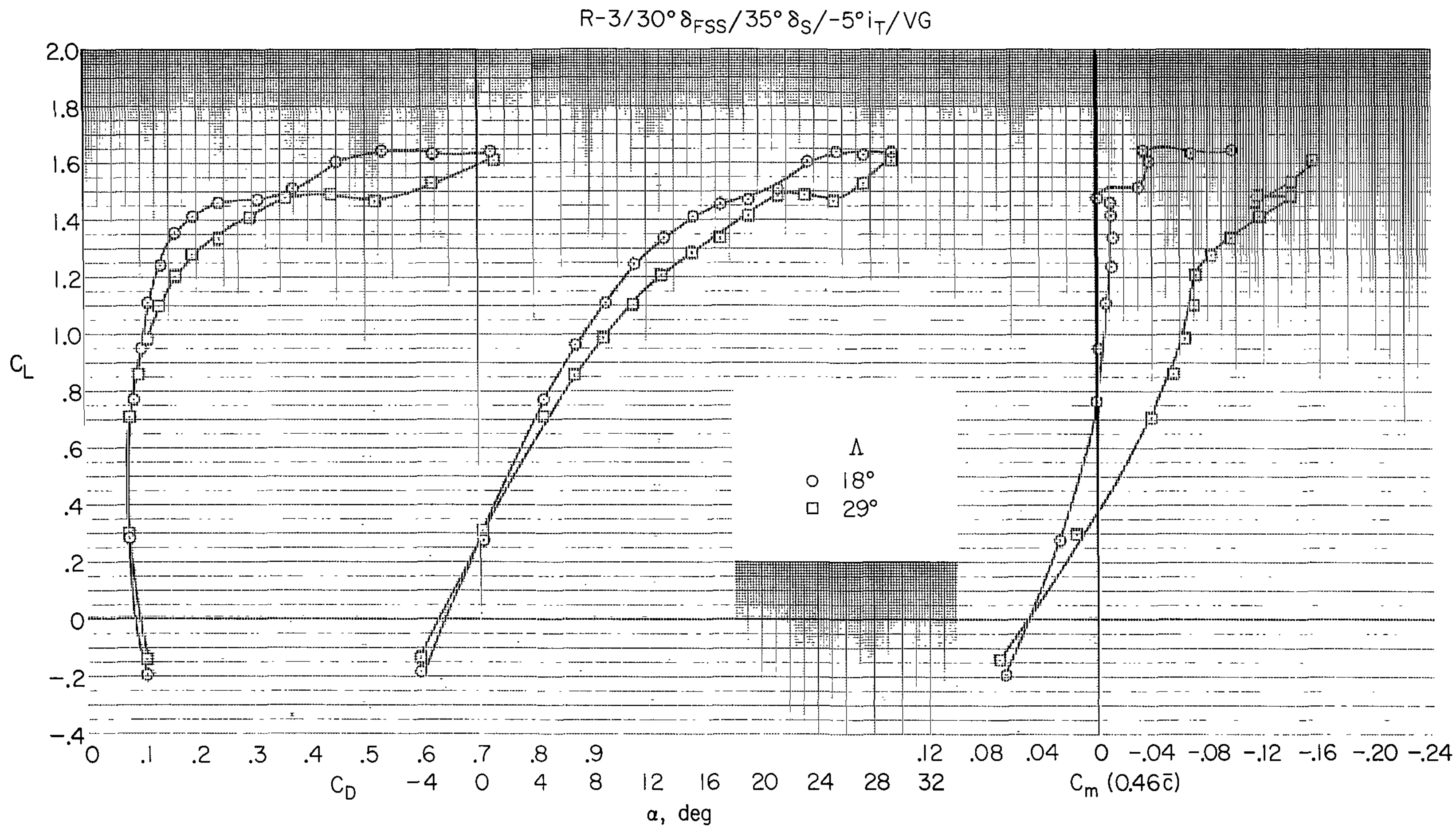

Figure 21.- Effect of wing sweepback angle, constant (large) radius strake leading edge, and vortex generators.

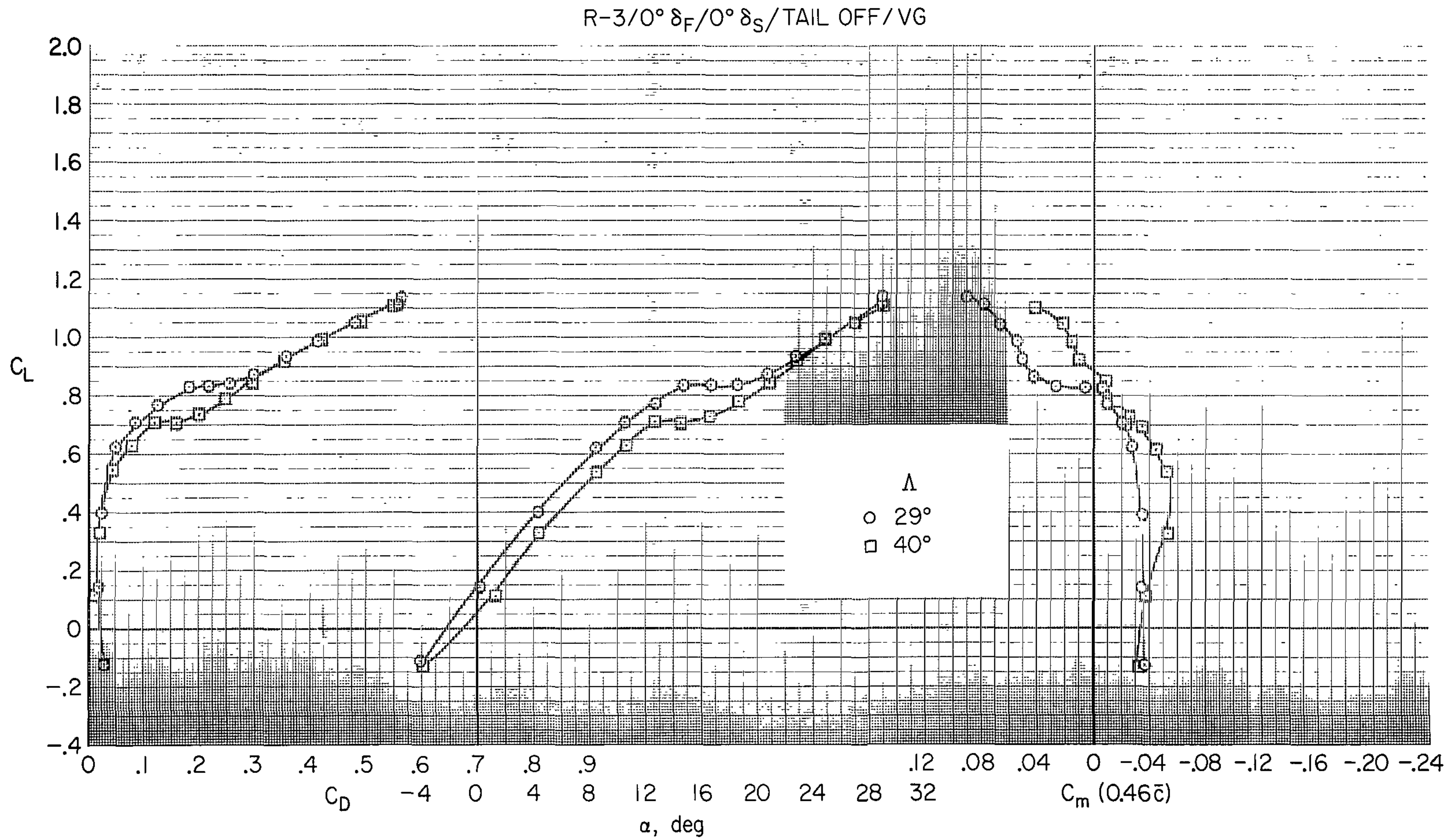

Figure 22.- Effect of wing sweepback angle, constant (large) radius strake leading edge, vortex generators, flaps and slats up, and tail off.

NASA-Langley, 1969 — 2 A-2600